Hepatitis B Virus X Protein Shifts Human Hepatic Transforming Growth Factor (TGF)-β Signaling from Tumor Suppression to Oncogenesis in Early Chronic Hepatitis B

Miki Murata,[1] Koichi Matsuzaki,[1] Katsunori Yoshida,[1] Go Sekimoto,[1] Yoshiya Tahashi,[1] Shigeo Mori,[1] Yoshiko Uemura,[2] Noriko Sakaida,[2] Junichi Fujisawa,[3] Toshihito Seki,[1] Kazuki Kobayashi,[4] Koutaro Yokote,[4] Kazuhiko Koike,[5] and Kazuichi Okazaki[1]

Hepatitis B virus X (HBx) protein is suspected to participate in oncogenesis during chronic hepatitis B progression. Transforming growth factor β (TGF-β) signaling involves both tumor suppression and oncogenesis. TGF-β activates TGF-β type I receptor (TβRI) and c-Jun N-terminal kinase (JNK), which differentially phosphorylate the mediator Smad3 to become C-terminally phosphorylated Smad3 (pSmad3C) and linker-phosphorylated Smad3 (pSmad3L). Reversible shifting of Smad3-mediated signaling between tumor suppression and oncogenesis in HBx-expressing hepatocytes indicated that TβRI-dependent pSmad3C transmitted a tumor-suppressive TGF-β signal, while JNK-dependent pSmad3L promoted cell growth. We used immunostaining, immunoblotting, and *in vitro* kinase assay to compare pSmad3L- and pSmad3C-mediated signaling in biopsy specimens representing chronic hepatitis, cirrhosis, or hepatocellular carcinoma (HCC) from 90 patients chronically infected with hepatitis B virus (HBV) with signaling in liver specimens from HBx transgenic mice. In proportion to plasma HBV DNA levels, early chronic hepatitis B specimens showed prominence of pSmad3L in hepatocytic nuclei. HBx-activated JNK/pSmad3L/c-Myc oncogenic pathway was enhanced, while the TβRI/pSmad3C/p21^{WAF1} tumor-suppressive pathway was impaired as human and mouse HBx-associated hepatocarcinogenesis progressed. Of 28 patients with chronic hepatitis B who showed strong oncogenic pSmad3L signaling, six developed HCC within 12 years; only one of 32 patients showing little pSmad3L developed HCC. In contrast, seven of 30 patients with little Smad3C phosphorylation developed HCC, while no patient who retained hepatocytic tumor-suppressive pSmad3C developed HCC within 12 years. *Conclusion:* HBx shifts hepatocytic TGF-β signaling from the tumor-suppressive pSmad3C pathway to the oncogenic pSmad3L pathway in early carcinogenic process. Hepatocytic pSmad3L and pSmad3C assessment in HBV-infected liver specimens should prove clinically useful for predicting risk of HCC. (HEPATOLOGY 2009;49:1203-1217.)

Hepatocellular carcinoma (HCC) is the fifth most common cancer worldwide and one of the most deadly, causing approximately 600,000 deaths yearly.[1] The overall incidence of HCC continues to rise, especially in western Europe and the United States.[2] During the past 20 years, striking advances have enhanced our understanding of HCC. More than 85% of HCC cases are related to known hepatitis B virus (HBV) and hepatitis C virus (HCV).

Abbreviations: Ab, antibody; HBV, hepatitis B virus; HBx, hepatitis B virus X; HCC, hepatocellular carcinoma; HCV, hepatitis C virus; HSC, hepatic stellate cells; IgG, immunoglobulin G; JNK, c-Jun N-terminal kinase; PPM1A, protein phosphatase magnesium 1A; pSmad3C, C-terminally phosphorylated Smad3; pSmad3L, linker-phosphorylated Smad3; SCP1-3, small C-terminal domain phosphatase 1-3; TGF-β, transforming growth factor β; TβRI, TGF-β type I receptor; TβRII, TGF-β type II receptor.

From the Departments of [1]Gastroenterology and Hepatology, [2]Surgical Pathology, and [3]Microbiology, Kansai Medical University, Osaka, Japan; the [4]Department of Clinical Cell Biology, Chiba University Graduate School of Medicine, Chiba, Japan; and the [5]Department of Infectious Diseases, Internal Medicine, Graduate School of Medicine, University of Tokyo, Tokyo, Japan.

Received March 19, 2008; accepted November 25, 2008.

Supported by the Ministry of Education, Science, and Culture of Japan (K. M.).

A strong correlation between chronic HBV infection and HCC occurrence has long been apparent according to epidemiologic evidence and the finding of integrated HBV DNA sequences in virtually all HBV-related HCC.[3] Hepatitis B virus X (HBx) oncoprotein has been implicated in HBV-mediated hepatocarcinogenesis,[4,5] and persistent high-level expression of HBx protein in transgenic mouse liver results in hyperplasia leading to HCC, with no preceding inflammation.[6] Although HBx does not bind DNA directly, HBx activates Ras/mitogen-activated protein kinase pathways including extracellular signal-regulated kinase and c-Jun N-terminal kinase (JNK),[7] resulting in tumor cell growth and survival.

Transforming growth factor β (TGF-β) can inhibit epithelial cell growth, acting as a tumor suppressor. During carcinogenesis, however, cancer cells gain advantage by selective reduction of the tumor-suppressive activity of TGF-β together with augmentation of its oncogenic activity.[8] This led us to hypothesize that alterations in the TGF-β signal transduction pathway could be involved in the development of HCC in long-standing HBV infection.

Smads are central mediators of signals from the receptors for TGF-β superfamily members to the nucleus.[9] Smads are modular proteins with conserved Mad-homology 1, intermediate linker, and Mad-homology 2 domains.[10] The catalytically active TGF-β type I receptor (TβRI) phosphorylates the C-terminal serine residues of receptor-activated Smads, which include Smad2 and the highly related protein Smad3. The linker domain can undergo regulatory phosphorylation by other kinases including mitogen-activated protein kinases and cyclin-dependent kinases.[11-14] In contrast to the clearly activating role of the C-terminal phosphorylation events, the regulation of Smad activity by phosphorylation of the linker region is complex. Linker phosphorylation of Smad2 during human colorectal carcinogenesis results in cytoplasmic retention of Smad2 and inhibition of tumor-suppressive TGF-β signaling.[11,15] However, Smad3 phosphorylated at the linker region (pSmad3L) is localized predominantly to cell nuclei in actively growing Ki-67–immunoreactive colon cancer with distant metastasis.[15] Reversible shifting of Smad-dependent signaling between tumor suppression and oncogenesis in hyperactive Ras-expressing cells indicates that Smad3 phosphorylated at the C-terminal region (pSmad3C) transmits a tumor-suppressive TGF-β signal, whereas oncogenic activities such as cell proliferation and invasion are promoted by the pSmad3L pathway.[16] In addition, Roberts' group[17] has recently reported that Smad3 is critical for Ras/JNK-mediated transformation. Taken together, these findings indicate that oncogenic TGF-β signaling results from the functional collaboration of Ras and Smad3 rather than from Ras-mediated inhibition of the Smad3 pathway. Linker phosphorylation of Smad3 indirectly inhibits C-terminal phosphorylation, minimizing tumor-suppressive pSmad3C signaling.[16] Notably, pSmad3L-mediated signaling in activated hepatic stellate cells (HSCs) promotes liver fibrosis by stimulating extracellular matrix deposition.[13,18]

The role of HBV and HCV in tumor formation appears to be complex and may involve both direct and indirect mechanisms.[19] Integration of HBV DNA into the host genome occurs at early steps of clonal tumor expansion. Alternatively, chronic liver inflammation and hepatic regeneration induced by host cellular immune responses can increase the risk of HCC development. During progression of HCV-related chronic liver disorders, hepatocytes affected by chronic inflammation undergo a transition from the tumor-suppressive pSmad3C pathway to the JNK/pSmad3L pathway.[20] Our present studies extend the previous observations to HBV-related hepatocarcinogenesis. We study Smad3 phosphorylation profiles in HBV-infected human liver and HBx transgenic mouse liver, concluding that HBx oncoprotein in early stages of chronic hepatitis B contributes directly to hepatocarcinogenesis by shifting hepatocytic Smad3-mediated signaling from tumor suppression to oncogenesis.

Patients and Methods

Patients, Follow-up, and Detection of HCC. Ninety patients with HBV-related chronic liver disease underwent liver biopsy at the Department of Gastroenterology and Hepatology of Kansai Medical University Hospital between 1992 and 1994. All patients were seropositive for hepatitis B surface antigen (Abbott Laboratories, North Chicago, IL) and were seronegative for anti-HCV antibody (Ortho Diagnostics, Tokyo, Japan). Patients included 70 with chronic hepatitis, 10 with cir-

Address reprint requests to: Koichi Matsuzaki, M.D., Departments of Gastroenterology and Hepatology, Kansai Medical University, 10-15 Fumizonocho, Moriguchi, Osaka, 570-8507, Japan. E-mail: matsuzak@takii.kmu.ac.jp; fax: (81)-6-6996-4874.

Published online in Wiley InterScience (www.interscience.wiley.com).

DOI 10.1002/hep.22765

Potential conflict of interest: Nothing to report.

Additional Supporting Information may be found on the online version of this article.

rhosis, and 10 with HCC. Sixty of the chronic hepatitis patients were enrolled in a program for early diagnosis of HCC; the other 10 were lost to follow-up. HBV DNA (Roche Diagnostics, Tokyo, Japan) and hepatitis B envelope antigen (Abbott Laboratories) were measured at the time of liver biopsy. During the surveillance period, patients were followed up with abdominal ultrasonography and plasma alpha-fetoprotein determinations every 3 to 6 months. We also made a random choice of 20 chronic hepatitis B specimens with little fibrosis (F1) and little inflammation (A1) from the liver biopsy specimens of the patients showing high plasma HBV DNA levels.

Necroinflammatory activity and fibrotic stage were graded histologically according to the classification of Desmet and colleagues.[21] We counted and scored pSmad3, HBx, and c-Myc positivity in hepatocytes as follows: 0, no positivity; 1, <25%; 2, 25% to 50%; 3, 50% to 75%; 4, >75%.[20] Written informed consent was obtained from each patient according to the Helsinki Declaration. We also obtained approval for this study from our institutional ethics committee.

Reverse-Transcription Polymerase Chain Reaction. Reverse-transcription polymerase chain reaction of TGF-β type II receptor (TβRII), Smad2, and Smad4 genes was performed as described.[15]

Domain-Specific Antibodies Against the Phosphorylated Smad3. Two polyclonal anti-phospho–Smad3 sera—α pSmad3L (Ser 208/213) and α pSmad3C (Ser 423/425)—were raised against the phosphorylated linker and C-terminal regions of Smad3 by immunization of rabbits with synthetic peptides. Relevant antisera were affinity-purified using phosphorylated peptides as described.[13]

Transgenic Animals. HBx transgenic mice were derived by microinjection of a 1151-bp HBV DNA fragment containing the HBx gene with its own regulatory elements and polyadenylation signal into fertilized eggs of CD-1 mice. An independent line (H9) was derived from founders.[6]

Immunohistochemical and Immunofluorescence Analyses. Immunohistochemical and immunofluorescence analyses were performed as described.[18] Primary antibodies (Abs) used in this study included mouse monoclonal anti-HBx Ab (2 μg/mL; Abcam, Cambridge, UK), mouse monoclonal anti-c-Myc Ab (10 μg/mL; Santa Cruz Biotechnology, Santa Cruz, CA), and mouse monoclonal anti-$p21^{WAF1}$ Ab (0.5 μg/mL; DAKO, Glostrup, Denmark), in addition to the affinity-purified rabbit polyclonal anti-pSmad3L (2 μg/mL) and anti-pSmad3C (0.5 μg/mL) as described above. Anti-pSmad3C Ab cross-reacted weakly with C-terminally phosphorylated Smad2: to block binding of anti-pSmad3C Ab to phosphorylated domains in Smad2, anti-pSmad3C Ab was adsorbed with 1 μg/mL C-terminally phosphorylated Smad2 peptide.

For immunohistochemical analyses, sections exposed to primary Abs were then incubated with peroxidase-labeled polymer conjugated to goat anti-mouse or anti-rabbit immunoglobulin G (IgG) (DAKO). Finally, sections were developed with 3,3'-diaminobenzidine tetrahydrochloride (DAB; Vector Laboratories, Burlingame, CA), counterstained with Mayer's hematoxylin (Merck, Darmstadt, Germany), and mounted under coverslips.

For double-labeling immunofluorescence analyses, sections exposed to a pair of primary Abs (rabbit plus mouse) were then incubated in a 1:500 dilution of goat anti-rabbit IgG conjugated with a red fluorophore (Alexa Fluor 594; Molecular Probes, Eugene, OR) and goat anti-mouse IgG conjugated with a green fluorophore (Alexa Fluor 488; Molecular Probes). Images were obtained with a fluorescence microscope (Carl Zeiss Microimaging, Oberkochen, Germany).

Immunoprecipitation and Immunoblotting. pSmad3L and pSmad3C immunoblots on Smad3 immunoprecipitates of cell extracts from frozen tissues representing either HCC or underlying liver diseases were performed as described.[20]

In Vitro *Kinase Assay.* *In vitro* kinase assay was performed as described.[12]

Statistical Analyses. The Kaplan-Meier method was used to determine the cumulative probability of appearance of HCC during the 12-year follow-up period. HCC occurrence curves were compared between patients with abundant (scores 3 to 4) and those with sparse (scores 0 to 2) Smad3L/C phosphorylation, by means of the log-rank test. For continuous variables, the optimal cutoff threshold for defining groups was established using receiver operating characteristics curves. All parameters with P values less than 0.10 in the univariate analysis were selected for multivariate analysis, which was performed using the Cox proportional hazards model.[22] P values less than 0.05 were considered significant. The Mann-Whitney U test was used to identify significant differences in hepatocytic pSmad3L and pSmad3C positivity among fibrotic stages.

Results

Two Distinct Hepatocytic Smad3 Signaling Pathways in Human Chronic Hepatitis B: pSmad3L- and pSmad3C-Dominant Types. We initially analyzed mutations of TβRII, Smad2, and Smad4 genes in 10 HCC and six cirrhotic liver samples, finding no mutations in

Table 1. Clinicopathologic Features, Smad3L/C Phosphorylation, and HBx and c-Myc Positivities in Specimens from Patients with HBV-Related Chronic Liver Disease

		Fibrotic Stage*				
	Nomal	F1	F2	F3	F4	HCC
Patients, n	2	20	27	23	10	10
Sex (male/female), n	2/0	13/7	19/8	17/6	5/5	10/0
Age (years), mean ± SD	57.0 ± 9.9	35.5 ± 14.3	34.3 ± 13.9	43.1 ± 13.7	59.6 ± 7.6	54.0 ± 15.1
pSmad3L staining, n†						
0	2	0	0	0	0	0
1	0	8	6	2	1	0
2	0	6	6	7	1	0
3	0	3	11	11	2	5
4	0	3	4	3	6	5
pSmad3C staining, n†						
0	0	0	0	0	0	0
1	0	0	4	4	2	4
2	0	4	9	12	7	3
3	2	11	7	5	1	3
4	0	5	7	2	0	0
Activity, n*						
A0	2	1	0	0	0	0
A1	0	17	6	1	0	1
A2	0	2	19	11	3	7
A3	0	0	2	11	7	2
HBx staining, n†						
0	2	0	0	0	1	1
1	0	6	5	3	2	3
2	0	7	11	8	3	3
3	0	3	7	6	2	2
4	0	4	4	6	2	1
c-Myc staining, n†						
0	2	0	0	0	0	0
1	0	2	4	1	1	0
2	0	9	10	8	3	1
3	0	6	8	8	3	3
4	0	3	5	6	3	6
Histology of HCC (well/moderate)‡						6/4
TNM stage (I/II/III/IV)ʃ						4/4/2/0
Size of tumor (cm), mean ± SD						2.2 ± 0.3
AST (IU/L), mean ± SD	22.5 ± 3.5	68.6 ± 56.1	92.8 ± 65.8	79.7 ± 51.8	82.0 ± 53.1	71.0 ± 36.4
ALT (IU/L), mean ± SD	24.0 ± 2.8	104 ± 83.5	141 ± 97.5	84.5 ± 83.1	68.2 ± 52.3	59.1 ± 32.2
Platelet count (× 10^9/L), mean ± SD	25.0 ± 4.2	17.1 ± 3.6	15.8 ± 4.9	14.1 ± 7.1	9.7 ± 6.7	9.0 ± 3.7
AFP (ng/mL), mean ± SD	2.1 ± 1.3	6.8 ± 4.6	14.8 ± 12.2	66.2 ± 138	132 ± 208	164 ± 184

Abbreviations: AFP, alpha-fetoprotein; ALT, alanine aminotransferase; AST, aspartate aminotransferase; pSmad3L, linker-phosphorylated Smad3; pSmad3C, C-terminally phosphorylated Smad3; SD, standard deviation; TNM, tumor-node-metastasis.

*Necroinflammatory activity and fibrotic stage are determined histologically according to Desmet's classification.

†Hepatocytic Smad3 phosphorylation is scored as follows: 0, no phosphorylation; 1, <25% Smad3 phosphorylation; 2, 25% to 50% Smad3 phosphorylation; 3, 50% to 75% Smad3 phosphorylation; 4, >75% Smad3 phosphorylation. Extent of HBx and c-Myc expression is indicated as that of pSmad3L positivity.

‡Histological grading of HCC is classified according to the criteria of the International Working Party.

ʃTNM is classified by the International Union Against Cancer and American joint Committee on Cancer.

any sample. This confirms the low probability of mutations in HCC tissues, which has been reported recently.[23]

To investigate domain-specific phosphorylation mediating Smad3 signaling *in vivo*, we generated two Abs specific to each phosphorylation site, and determined the distribution of pSmad3L and pSmad3C in chronic hepatitis B and C specimens. Table 1 shows clinical background and positivity for pSmad3L and pSmad3C in 90 patients with HBV-related chronic liver diseases. We also studied HCC occurrence over 12 years in 60 patients with chronic hepatitis B who were enrolled in a program for early diagnosis of HCC (Table 2). We recently reported that Smad3 was phosphorylated at the linker region, particularly in groups of hepatocytes adjoining collagen fibers in portal tracts in chronic hepatitis C.[20] In contrast, the distribution of pSmad3L and pSmad3C in chronic

Table 2. Clinicopathologic Features, Smad3L/C Phosphorylation, and HCC Incidence in Specimens from Patients with HBV-Related Chronic Hepatitis

Patient No.	Sex	Age	Incidence of HCC	pSmad3L Staining*	pSmad3C Staining*	Fibrotic Stage†	Inflammatory Activity†	HBV DNA (log copies/mL)	HBeAg
1	M	62	○	4	2	3	3	5.4	+
2	F	44	○	4	2	2	2	5.5	−
3	M	22	○	4	2	2	2	5.2	−
4	F	20		4	4	3	3	3.0	−
5	M	43		4	4	2	2	4.5	−
6	M	30		4	2	2	3	4.0	−
7	M	30		4	2	2	3	5.6	−
8	M	65	○	3	2	3	3	4.0	+
9	F	56	○	3	2	3	2	3.7	+
10	M	52	○	3	1	1	1	6.4	−
11	F	40		3	1	1	1	6.9	−
12	M	44		3	1	3	3	5.1	−
13	M	45		3	1	3	3	3.8	−
14	M	28		3	2	3	1	3.0	−
15	M	60		3	2	3	2	2.8	−
16	M	44		3	2	3	3	5.2	+
17	M	44		3	2	3	3	3.2	+
18	M	44		3	2	3	3	4.4	−
19	F	26		3	2	2	1	4.9	−
20	M	20		3	2	2	1	2.9	+
21	M	59		3	2	2	2	4.4	−
22	M	43		3	3	2	2	3.2	+
23	M	29		3	3	3	2	6.2	−
24	M	29		3	3	3	2	3.0	−
25	M	25		3	4	1	1	3.5	−
26	F	33		3	4	2	2	4.6	+
27	M	19		3	3	3	2	5.6	−
28	M	63		3	4	2	2	5.1	−
29	M	52	○	2	1	3	2	3.7	−
30	M	44		2	2	3	3	5.2	−
31	M	29		2	2	3	2	3.9	+
32	F	46		2	4	3	3	3.2	−
33	M	25		2	2	1	2	5.0	−
34	F	23		2	3	1	1	2.1	−
35	F	31		2	3	2	2	3.9	+
36	F	26		2	3	1	1	2.4	−
37	M	35		2	3	1	1	5.6	−
38	M	20		2	3	2	1	3.2	+
39	F	56		2	3	3	2	5.1	+
40	F	36		2	3	3	2	2.6	−
41	F	25		2	3	2	1	5.1	−
42	F	23		2	4	2	1	3.5	−
43	F	41		2	4	1	1	2.0	+
44	M	29		2	4	2	2	4.5	−
45	M	31		2	4	1	1	5.9	+
46	M	42		2	1	2	2	3.7	−
47	M	24		1	1	2	2	3.9	+
48	M	28		1	2	3	2	3.8	−
49	F	11		1	2	2	2	3.0	+
50	M	40		1	1	2	2	3.2	−
51	M	37		1	2	2	2	3.0	−
52	F	10		1	2	2	2	2.3	−
53	M	16		1	3	1	1	5.1	−
54	M	41		1	3	1	1	4.3	−
55	M	40		1	3	1	1	2.2	−
56	M	53		1	3	1	1	2.7	−
57	M	27		1	3	1	1	4.6	−
58	M	53		1	4	1	1	3.3	−
59	M	30		1	4	2	2	2.1	−
60	F	22		1	4	1	0	3.7	−

Abbreviations: F, female; HBeAg, hepatitis B e antigen; HBV, hepatitis B virus; HCC, hepatocellular carcinoma; M, male; pSmad3C, C-terminally phosphorylated Smad3; pSmad3L, linker-phosphorylated Smad3.

*Hepatocytic Smad3 phosphorylation is scored as follows: 0, no phosphorylation; 1, <25% Smad3 phosphorylation; 2, 25% to 50% Smad3 phosphorylation; 3, 50% to 75% Smad3 phosphorylation; 4, >75% Smad3 phosphorylation.

†Necroinflammatory activity and fibrotic stage are determined histologically according to Desmet's classification.

hepatitis B specimens was divided into two distinct patterns. In one liver specimen with moderate fibrosis and inflammation from patient 2 in Table 2 who was diagnosed with HCC 9 years later, intense pSmad3L immunostaining was present in the nuclei of all hepatocytes throughout the liver lobules; C-terminal phosphorylation of Smad3 was strongly suppressed in hepatocytic nuclei (Fig. 1A and Supplementary Fig. 1). In another specimen with similar fibrotic stage and necroinflammatory activity from patient 44 in Table 2 who had not developed HCC, many hepatocytes retained phosphorylation at Smad3C but showed scarce phosphorylation at Smad3L (Fig. 1B). Among 37 patients with chronic hepatitis B who had strong pSmad3L positivity, 24 patients showed little Smad3C phosphorylation, and only 13 patients showed abundant Smad3C phosphorylation (64.9% versus 35.1% [$P = 0.03$]) (Table 3). In contrast, 22 patients with little Smad3L phosphorylation (scores 0 to 2) versus only 13 patients with abundant Smad3L phosphorylation (scores 3 to 4) showed strong pSmad3C positivity (62.9% versus 37.1% [$P = 0.04$]). Because the extent of Smad3L phosphorylation increased as fibrotic stage and necroinflammatory activity progressed in chronic hepatitis C, Smad3L showed little phosphorylation in early chronic hepatitis C.[20] In contrast, degree of linker phosphorylation of Smad3 in hepatocytic nuclei remained high (staining scored as 3 or 4) in 21 of 47 patients with chronic hepatitis B (F1 to F2) (Fig. 1C). These results indicate differential mechanisms of HBV- and HCV-

Table 3. Correlation Between pSmad3L and pSmad3C in Chronic Hepatitis B Specimens

	pSmad3C Positivity *		
	Low (1 and 2)	High (3 and 4)	Total
pSmad3L positivity *			
Low (1 and 2)	11	22	33
High (3 and 4)	24	13	37
Total	35	35	70

Abbreviations: pSmad3C, C-terminally phosphorylated Smad3; pSmad3L, linker-phosphorylated Smad3.

*Hepatocytic Smad3 phosphorylation is scored as follows: 0, no phosphorylation; 1, <25% Smad3 phosphorylation; 2, 25% to 50% Smad3 phosphorylation; 3, 50% to 75% Smad3 phosphorylation; 4, >75% Smad3 phosphorylation.

COLOR

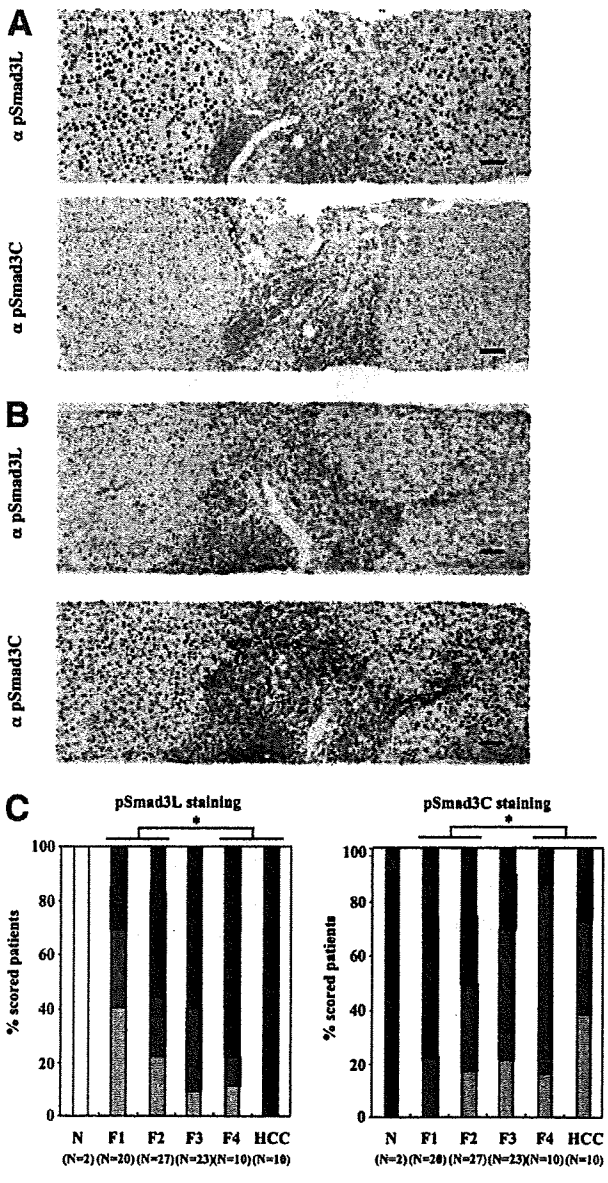

Fig. 1. Two distinct hepatocytic Smad3 signaling pathways in early chronic hepatitis B: pSmad3L- and pSmad3C-dominant types. (A) Smad3 in the nuclei of hepatocytes was phosphorylated sparsely at the C-terminal region (α pSmad3C column) but intensely at the linker region (α pSmad3L column). The liver specimen showing moderate fibrosis and inflammation was obtained from patient 2 in Table 2 diagnosed with HCC 9 years later. Bar = 50 μm. (B) In patient 44 in Table 2 who had not developed HCC, hepatocytes retained phosphorylation at Smad3C (α pSmad3C column) but showed little phosphorylation at Smad3L (α pSmad3L column). The specimen showed degrees of fibrosis and necroinflammatory activity similar to those in (A). Formalin-fixed, paraffin-embedded liver sections were stained with anti-pSmad3L Ab (α pSmad3L column) and anti-pSmad3C Ab (α pSmad3C column). The pSmad3C section was paired with an adjacent section stained using anti-pSmad3L Ab. Abs were then bound by goat anti-rabbit IgG conjugated with peroxidase-labeled polymer. Peroxidase activity was detected with 3,3'-diaminobenzidine tetrahydrochloride. All sections were counterstained with hemotoxylin (blue). Brown color indicates specific Ab reactivity. Bar = 50 μm. (C) Degrees of Smad3 phosphorylation were stable in hepatocytic nuclei in early chronic hepatitis B specimens (F1 to F2), whereas pSmad3L increased and pSmad3C decreased as chronic hepatitis B (F3) progressed through cirrhosis to HCC. Smad3 phosphorylation in hepatocytes did not change between F1 and F2 stages. Phosphorylation of Smad3L and Smad3C in hepatocytes of cirrhotic liver (F4) and HCC was greater and less than that in livers with grade F1 and F2 fibrosis, respectively. Extent of Smad3 phosphorylation: □, 0; □, 1; ▩, 2; ■, 3; ■, 4. *$P < 0.05$.

associated carcinogenesis, especially in the early stages of chronic hepatitis.

pSmad3L Prominence in Hepatocytic Nuclei in Proportion to Plasma HBV DNA Levels. Because HCC risk is related to plasma HBV DNA levels and chronic inflammation,[24] we next investigated the correlation of hepatocytic pSmad3L positivity with plasma HBV DNA levels and necroinflammatory activity in chronic hepatitis B patients (Fig. 2). Positivity of hepatocytic nuclei for pSmad3L in chronic hepatitis B specimens gradually increased in proportion to amounts of HBV DNA.

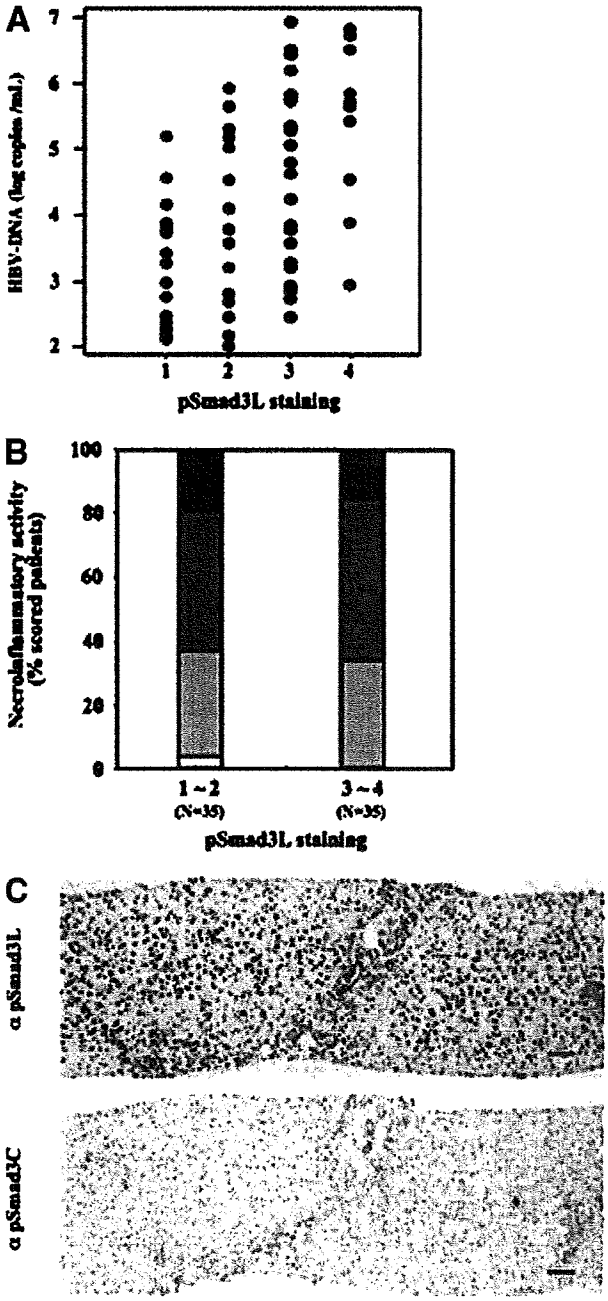

Sixteen sera samples of 35 patients with abundant Smad3L phosphorylation (scores 3 to 4) but only seven sera samples of 35 patients with little Smad3L phosphorylation (scores 0 to 2) contained more than 5.0 log copies/mL (45.7% versus 20.0% [$P = 0.02$]) (Fig. 2A). However, 23 of 35 chronic hepatitis B patients with abundant Smad3L phosphorylation and 22 of 35 patients with little Smad3L phosphorylation showed a high level of inflammatory activity (A 2 to 3) (65.7% versus 62.9% [$P = 0.80$]) (Fig. 2B). These results indicated that HBV itself could up-regulate the hepatocytic phosphorylation at Smad3L, but inflammation could not strongly affect linker phosphorylation.

To further confirm the direct effects of HBV, besides chronic inflammation, on phosphorylation at Smad3L in early chronic hepatitis B, we examined the degrees of pSmad3L and pSmad3C in a group of patients with little fibrosis (F1), little inflammation (A1), and high plasma HBV DNA. Smad3L was highly phosphorylated in hepatocytic nuclei, whereas the phosphorylation at Smad3C was suppressed (Fig. 2C). Of 20 chronic hepatitis B samples, 12 samples showed abundant Smad3L phosphorylation (scores 3 to 4), but only five samples had abundant Smad3C phosphorylation (60.0% versus 25.0% [$P = 0.03$]) (Table 4).

HBx Protein Involvement in c-Myc–Mediated Oncogenic Activity via the pSmad3L Pathway in Human Chronic Hepatitis B. Integrated viral sequences produce HBx protein, which brings about up-regulation of c-Myc oncoprotein.[25] We therefore investigated whether HBx protein affected Smad3L phosphorylation and expression of c-Myc in biopsy specimens from HBV-infected livers by immunostaining sections for

Fig. 2. In proportion to plasma HBV DNA levels, JNK-dependent pSmad3L became prominent in the nuclei of hepatocytes in human early chronic hepatitis B. (A) Positivity for pSmad3L in hepatocytic nuclei in chronic hepatitis B specimens was greater in proportion to plasma HBV DNA levels. Patients with strong pSmad3L positivity in hepatocytic nuclei (staining scored as 3 or 4) had more HBV DNA in plasma than patients with weak pSmad3L positivity (staining scored as 0 to 2). Hepatocytic Smad3 phosphorylation in chronic hepatitis B specimens is scored as follows: 0, no phosphorylation; 1, <25%; 2, 25% to 50%; 3, 50% to 75%; 4, >75%. (B) Degree of Smad3 phosphorylation at the linker region did not strongly correlate with necroinflammatory activity of chronic hepatitis B. Hepatocytic Smad3 phosphorylation at the linker region in livers with necroinflammatory activities of A2 to A3 was essentially similar to phosphorylation in those with activities of A0 to A1. Extent of necroinflammatory activity: □, 0; □, 1; ▩, 2; ■, 3. (C) Smad3 in the nuclei of hepatocytes was phosphorylated intensely at linker region (α pSmad3L column) but sparsely at the C-terminal region (α pSmad3C column). The liver specimen showing minimal fibrosis (F1) and inflammation (A1) was obtained from patient 10 in Table 2 who showed high plasma HBV DNA and was diagnosed with HCC 4 years later.

Table 4. Clinicopathologic Features, Smad3L/C Phosphorylation, and Plasma HBV DNA Levels in Specimens from Patients with Early Chronic Hepatitis B

Patient No.	Sex	Age	pSmad3L staining*	pSmad3C staining*	Fibrotic Stage†	Inflammatory Activity†	HBV DNA (log copies/mL)
1	M	46	4	2	1	1	5.6
2	M	45	4	2	1	1	5.4
3	F	38	3	1	1	1	6.2
4	F	49	3	1	1	1	5.2
5	F	52	3	1	1	1	6.1
6	F	40	3	2	1	1	5.8
7	F	28	3	2	1	1	5.6
8	M	38	3	2	1	1	5.5
9	M	44	3	2	1	1	5.3
10	F	40	3	2	1	1	5.4
11	M	55	3	2	1	1	5.1
12	F	43	3	3	1	1	5.8
13	M	34	2	1	1	1	5.2
14	M	28	1	1	1	1	5.2
15	F	35	1	2	1	1	5.1
16	M	30	1	2	1	1	5.3
17	M	45	1	3	1	1	5.2
18	M	38	1	4	1	1	5.6
19	M	54	1	4	1	1	5.2
20	M	48	1	4	1	1	5.4

Abbreviations: F, female; HBV, hepatitis B virus; M, male; pSmad3C, C-terminally phosphorylated Smad3; pSmad3L, linker-phosphorylated Smad3.

*Hepatocytic Smad3 phosphorylation is scored as follows: 0, no phosphorylation; 1, <25% Smad3 phosphorylation; 2, 25% to 50% Smad3 phosphorylation; 3, 50% to 75% Smad3 phosphorylation; 4, >75% Smad3 phosphorylation.

†Necroinflammatory activity and fibrotic stage are determined histologically according to Desmet's classification.

pSmad3L, paired with sections immunostained for HBx and c-Myc.

In specimens from patient 3 in Table 2 with chronic hepatitis B, pSmad3L, HBx, and c-Myc were distributed in hepatocytes throughout liver lobules (Fig. 3A and Supplementary Fig. 2). Double immunofluorescence studies in chronic hepatitis B specimens confirmed that pSmad3L was colocalized in HBx- and c-Myc–immunoreactive hepatocytes (Fig. 3B). HBx and c-Myc expression increased in hepatocytes of hepatitis B specimens as Smad3 showed more phosphorylation at the linker region (Fig. 3C).

Increased JNK/pSmad3L/c-Myc Oncogenic Signaling and Impaired pSmad3C/p21 ^{WAF1} Tumor-Suppressive Signaling as Chronic Hepatitis B Progresses From Cirrhosis to HCC. We further investigated tumor-suppressive and oncogenic Smad3 signaling in biopsy specimens during HBV-related hepatocarcinogenesis by staining sections using anti-pSmad3L Ab and anti-pSmad3C Ab, paired with sections stained for anti–c-Myc Ab and anti-p21^{WAF1} Ab. Although pSmad3L accelerates tumor growth by up-regulating c-Myc, pSmad3C participates in tumor suppression by up-regulating p21^{WAF1} transcription.[16, 20]

In specimens from a patient with chronic hepatitis B, the distribution of pSmad3L fit well with the pattern shown by c-Myc immunolabeling (Fig. 4A, chronic hepatitis panel): both were strong in hepatocytes throughout liver lobules. Linker phosphorylation and c-Myc staining increased further as chronic liver disease progressed through cirrhosis to HCC (Fig. 4A, cirrhosis and HCC panels).

Distribution of pSmad3C resembled the pattern obtained by p21^{WAF1} staining in chronic hepatitis B specimens (Fig. 4B, chronic hepatitis panel). As with pSmad3C distribution, hepatocytes showed increased p21^{WAF1} staining in nuclei. In contrast to intense staining for pSmad3L and c-Myc, pSmad3C and p21^{WAF1} staining decreased in hepatocytic nuclei in cirrhotic liver (Fig. 4B, cirrhosis panel). Nuclear pSmad3C and p21^{WAF1} immunostaining showed only a scattered distribution throughout HCC specimens (Fig. 4B, HCC panel). Semiquantitative analyses of positivity for pSmad3L, pSmad3C, and c-Myc in HBV-related chronic liver disease showed increasing pSmad3L/c-Myc and decreasing pSmad3C as chronic hepatitis B progressed from cirrhosis (F4) to HCC (Table 1).

We next quantified the extent of phosphorylation at Smad3L and Smad3C by immunoblotting with domain-specific Abs against phosphorylated Smad3 in tissue samples representing various stages of HBV-related chronic liver disorders. The linker region of Smad3 showed very little phosphorylation in normal liver (Fig. 4C, α pSmad3L panel). Remarkable up-

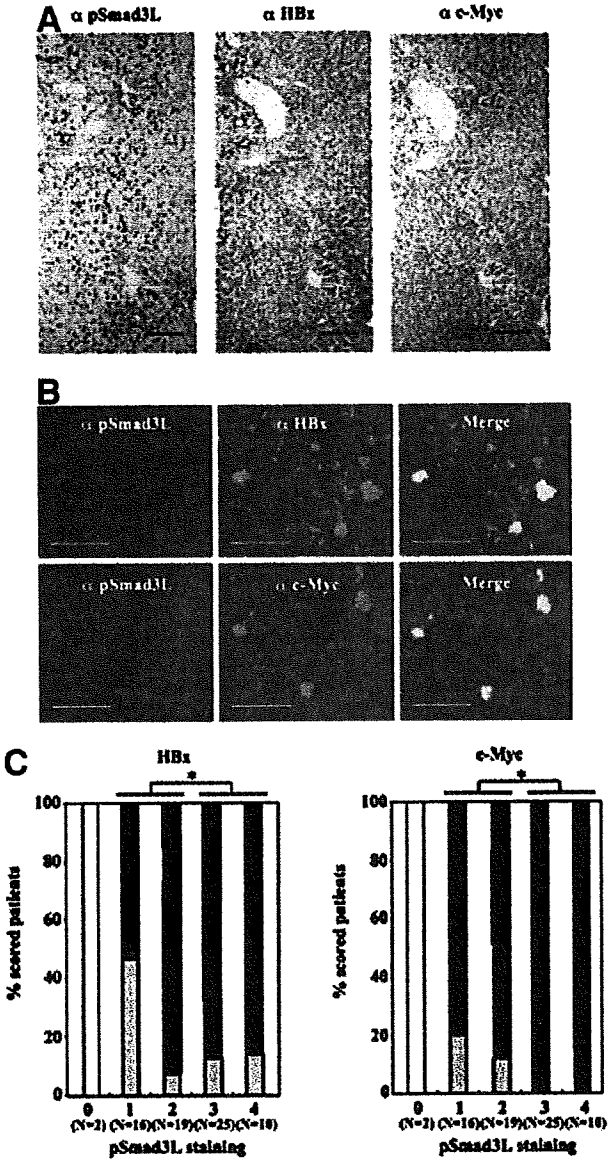

Fig. 3. HBx might be involved in c-Myc-mediated oncogenic activity in human chronic hepatitis B via the pSmad3L pathway. (A) Hepatocytes of chronic hepatitis B specimens from patient 3 in Table 2 showed diffuse immunostaining for pSmad3L, HBx, and c-Myc. All sections were counterstained with hemotoxylin (blue). Brown color indicates specific Ab reactivity. Bar = 50 μm. (B) pSmad3L in hepatocytic nuclei of chronic hepatitis B specimens was colocalized with HBx and c-Myc proteins. Sections of chronic hepatitis B tissues were stained for immunofluorescence to simultaneously detect pSmad3L (red) and HBx or c-Myc (green). Yellow color indicates overlap of proteins. Hepatocytes immunoreactive for pSmad3L showed colocalization of HBx (upper column) and c-Myc (lower column). Bar = 50 μm. (C) HBx and c-Myc expression increased in hepatocytes of chronic hepatitis B specimens as Smad3 was increasingly phosphorylated at the linker region. HBx and c-Myc expression was greater in hepatocytes with high phosphorylation at Smad3L (staining scored as 3 or 4) than in hepatocytes with staining scored as 0 to 2. The extent of HBx and c-Myc expression is indicated as that of pSmad3L positivity: □, 0; □, 1; ▩, 2; ■, 3; ■, 4. *$P < 0.05$.

regulation of pSmad3L was seen with progression of hepatic fibrosis and carcinogenesis. In cirrhotic liver and HCC, pSmad3L was far more abundant than in chronic hepatitis. In contrast, pSmad3C gradually decreased as disease stages progressed toward HCC (Fig. 4C, α pSmad3C panel).

We previously reported that Smad3L served as a substrate for JNK.[12] To address the functional relationship between activated JNK and Smad3L phosphorylation during hepatocarcinogenesis, we presently assayed kinase activity *in vitro*. Although JNK from normal liver showed little ability to phosphorylate Smad3 at the linker region, JNK from livers involved by chronic hepatitis B, cirrhosis, and HCC could directly phosphorylate Smad3L (Fig. 4D). These results suggested that JNK in preneoplastic liver tissues and HCC directly phosphorylated the linker region of Smad3.

Collectively, JNK/pSmad3L/c-Myc onogenic signaling in hepatocytes came to predominate while the tumor-suppressive pSmad3C/p21^{WAF1} pathway became quiescent as chronic hepatitis B progressed to cirrhosis and then HCC.

Selective Blockade of Linker Phosphorylation Abolishes pSmad3L-Mediated Cell Growth in HBx-Expressing Hepatocytes. pSmad3L, HBx, and c-Myc were colocalized in preneoplastic lesions including chronic hepatitis and cirrhosis (Fig. 3). These findings suggest that HBx oncoprotein might alter hepatocytic TGF-β signaling in chronic hepatitis B. We investigated this hypothesis using HBx-expressing hepatocytes. Selective blockade of linker phosphorylation by a mutant Smad3 lacking the JNK-dependent linker phosphorylation sites abolished pSmad3L-mediated cell growth in HBx-expressing hepatocytes (Supplementary Figs. 3-5). These results suggest that HBx activated the JNK/pSmad3L pathway, further promoting cell proliferation by up-regulating c-Myc transcription (Fig. 5).

Activation of the pSmad3L/c-Myc Pathway as HBx Transgenic Mouse Livers Progress Through Hyperplasia to HCC. We further investigated localization of pSmad3L, HBx, and c-Myc during HBx-induced hepatocarcinogenesis in HBx transgenic mouse livers. Beginning at the age of 2 months, HBx transgenic mouse liver showed centrilobular foci of cellular alteration with cytoplasmic vacuolation surrounding the central veins where bromodeoxyuridine was uptaken into the hepatocytes.[6]

In this hyperplastic mouse liver, phosphorylation at Smad3L was observed in hepatocytic nuclei in the centrilobular region, and distribution of pSmad3L was similar to those of HBx and c-Myc (Fig. 6A). pSmad3L, HBx,

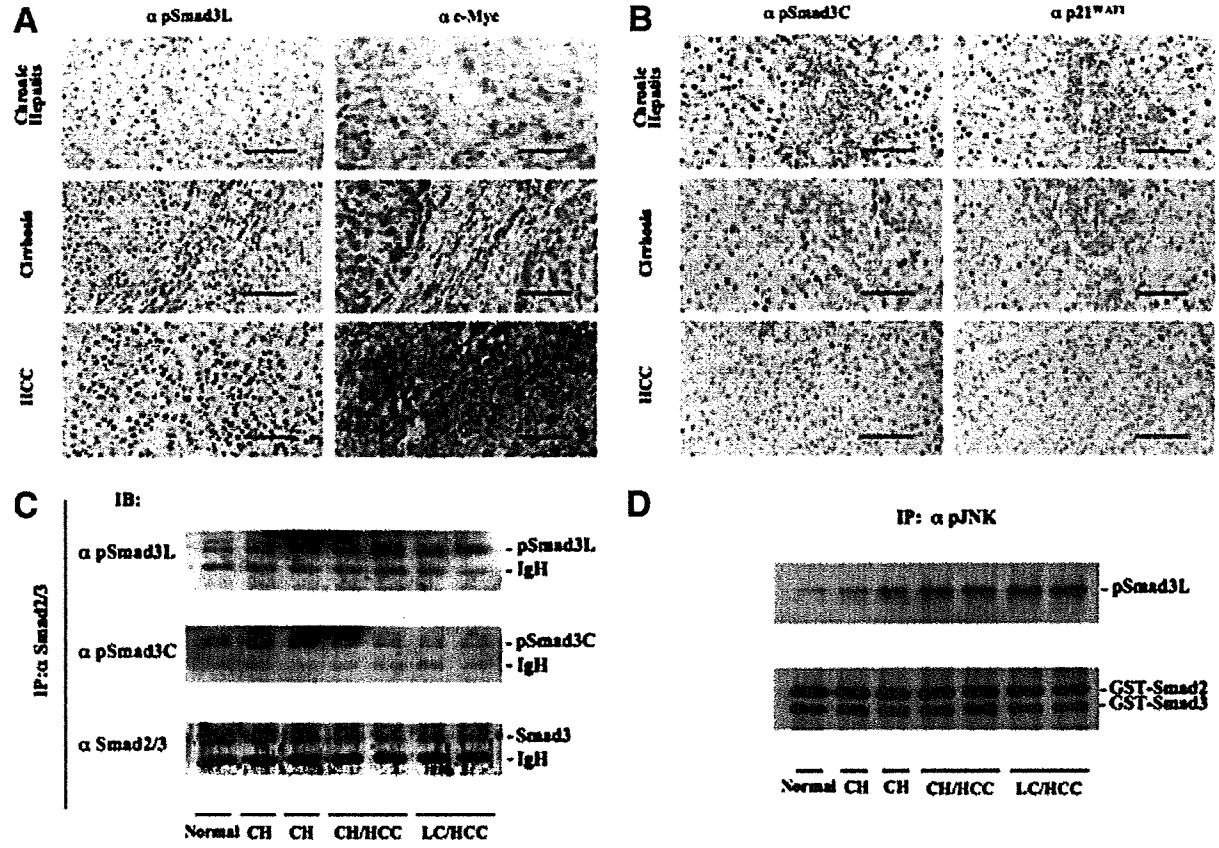

Fig. 4. As chronic hepatitis B progressed through cirrhosis to HCC, JNK/pSmad3L/c-Myc ongogenic signaling started to increase, whereas the tumor-suppressive pSmad3C/p21^{WAF1} pathway decreased. (A) pSmad3L and c-Myc increased as human chronic hepatitis B progressed through cirrhosis to HCC. (B) pSmad3C and p21^{WAF1} decreased as human chronic hepatitis B progressed through cirrhosis to HCC. All sections in A and B were counterstained with hemotoxylin (blue). Brown staining indicates specific Ab reactivity. Bar = 50 μm. (C) Immunoblotting of pSmad3L and pSmad3C in HBV-related chronic liver diseases. Cell lysates obtained from hepatocellular carcinoma (HCC) and surrounding nonneoplastic liver tissues including chronic hepatitis B (CH) or liver cirrhosis (LC) as well as uninvolved normal liver tissues from a patient with a metastatic liver tumor were subjected to anti-Smad3 immunoprecipitation (IP) and were then immunoblotted with each anti-pSmad3 Ab (upper panels). Relative amounts of endogenous Smad3 were determined via immunoblotting using anti-Smad3 Ab (bottom panel). (D) JNK in human HBV-related chronic liver tissue directly phosphorylated Smad3 at the linker region. Cell lysates obtained from HCC and surrounding nonneoplastic liver tissue including chronic hepatitis (CH) and liver cirrhosis (LC) from HBV-infected patients, as well as uninvolved normal liver tissue from a patient with a liver metastasis, were subjected to anti-phospho-JNK1/2 immunoprecipitation (IP), and were then mixed with bacterially expressed GST-Smad3 and GST-Smad2. After *in vitro* kinase assay, phosphorylation of Smad3L was analyzed via immunoblotting using anti-pSmad3L antibody (upper panel). Total Smad3 and Smad2 were determined via immunoblotting using anti-Smad2/3 Ab (lower panel).

and c-Myc were distributed diffusely in HCC specimens (Fig. 6B, HCC panel). Semiquantitative analyses of positivity for these molecules in HBx transgenic mouse livers also revealed that hepatocytic pSmad3L, HBx, and c-Myc increased as mouse liver progressed through hyperplasia to HCC (Fig. 6C). Double immunofluorescence studies in hyperplastic specimens confirmed that pSmad3L was colocalized in HBx- and c-Myc-immunoreactive hepatocytes (Fig. 6D).

Success in comparative study of HBx, pSmad3L, and c-Myc positivity during human and mouse hepatocarcinogenesis identified pSmad3L as a key regulatory element that offers a general framework for understanding the origins of HBV-related HCC.

Chronic Hepatitis B Patients with Hepatocytes Positive for pSmad3L and Negative for pSmad3C Increased Risk of HCC Development. We finally investigated whether phosphorylation levels of Smad3 could affect the risk of neoplastic evolution in the patients with chronic hepatitis B (Table 2). To compare HCC incidence, patients were classified into those with abundant (scores 3 to 4) and limited (scores 0 to 2) Smad3 phosphorylation in hepatocytic nuclei. HCC developed in six of 28 patients with abundant Smad3L phosphory-

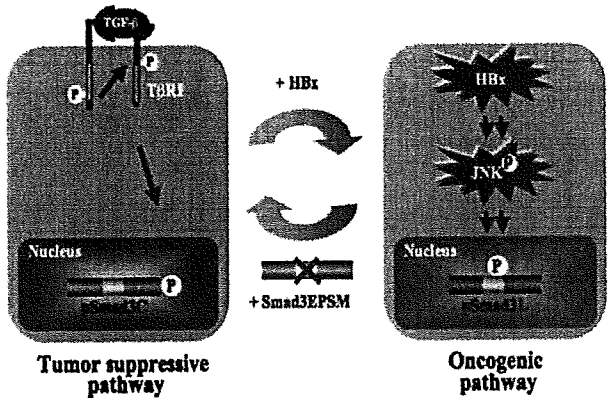

Fig. 5. Reversibility of Smad3-dependent signaling between tumor suppression and oncogenesis in HBx-expressing hepatocytes. Hepatocytes exhibit TGF-β-dependent Smad3 phosphorylation at the C-terminal region, which results in growth inhibition by repression of c-Myc. High expression of HBx protein in hepatocytes tends to shut down pSmad3C-mediated signaling and favor acquisition of constitutively active JNK-mediated pSmad3L signaling, which fosters cell growth by up-regulating c-Myc. Selective blockade of linker phosphorylation by a mutant Smad3 lacking the JNK-dependent linker phosphorylation sites (Smad3EPSM) restores the TGF-β-dependent tumor-suppressive response involving pSmad3C that is shown by parental hepatocytes.

lation, but in only one of 32 patients with limited Smad3L phosphorylation (log-rank = 0.03) (Fig. 7A). In contrast, HCC developed only in the patients with limited Smad3C phosphorylation, and no patients with abundant hepatocytic pSmad3C developed HCC (log-rank = 0.009) (Fig. 7B).

Several studies have analyzed risk factors for HCC occurrence in patients with HBV-related chronic liver disease, including elevated plasma HBV DNA[24] and seropositivity for hepatitis B e antigen.[26] In the univariate analysis, HCC occurrence in high pSmad3L positivity ($P = 0.01$), low pSmad3C positivity ($P = 0.03$), and plasma HBV-DNA levels of more than 5.0 log copies/mL ($P = 0.05$) showed P values less than 0.10, thus being significantly associated with HCC (Table 5). All variables with statistical significance in the univariate analysis were entered in the multivariate analysis, and high pSmad3L and low pSmad3C positivity were considered significantly predictive of HCC development within 12 years. Hepatocytic positivitiy for pSmad3L and pSmad3C should allow us to distinguish chronic hepatitis B patients at high and low risk for the development of HCC in near future.

Discussion

In patients with chronic hepatitis B, persistent HBV infection is clearly the primary inducer of HCC.[1-7] Comparative studies that seek to identify conserved oncogenic signaling common to HCC in both humans and experimental animals will help to eventually identify the molecular pathways that drive the development of HCC.[27] Much is known about the morphologic changes of cells and tissues that precede and accompany development of HCC in humans, allowing earlier diagnosis in some instances.[28] A variety of molecular alterations have been detected in fully developed HCC and to a lesser extent in morphologically defined preneoplastic precursor lesions.[29] Our current studies compared pSmad3L- and pSmad3C-mediated signaling in biopsy specimens of chronic hepatitis, cirrhosis, or HCC from 90 patients with chronic HBV infection versus signaling in preneoplastic and neoplastic liver lesions of HBx transgenic mice. Taken together with the results of *in vitro* experiments using HBx-expressing hepatocytes, our findings indicate that the HBx oncoprotein participates directly in hepatocarcinogenesis by shifting hepatocytic Smad3-mediated signaling from tumor suppression to oncogenesis in patients with early chronic hepatitis B (Fig. 7C). According to the two-step model of carcinogenesis (initiation and promotion), tumor formation can be explained by permanent HBx-dependent activation of the JNK/pSmad3L cascade that has a tumor promoter-like action.

HCC is a human neoplasm associated with viral infection.[1,3] At present, hepatitis virus–associated carcinogenesis can be seen as a multifactorial process that includes both direct and indirect mechanisms.[19] A major factor in the process of HCC development is the host immune system.[30] Chronic inflammation, degeneration, and regeneration induced by the host cellular immune response are common to a variety of human liver diseases, and subsequent cellular proliferation might increase the risk of cancer. We previously reported that increased phosphorylation of Smad3L and decreased phosphorylation of Smad3C were associated with an increased risk of HCV-related HCC.[20] Similarly to HCV-related chronic liver disease, strong pSmad3L positivity was observed in the late stages of HBV-related chronic liver disease (F3 to F4) (Fig. 1C). Considering the development of HCC in HCV core gene-transgenic mice,[31] hepatitis viruses themselves together with the host immune response might promote human hepatocarcinogenesis via the JNK/pSmad3L pathway during the late stage of the carcinogenic process in both HBV- and HCV- related chronic liver disease.

However, HBV and HCV have different roles in human hepatocarcinogenesis when early chronic hepatitis (F1 to F2) is considered. The histological severity of-HCV-related liver disease correlates closely with the risk

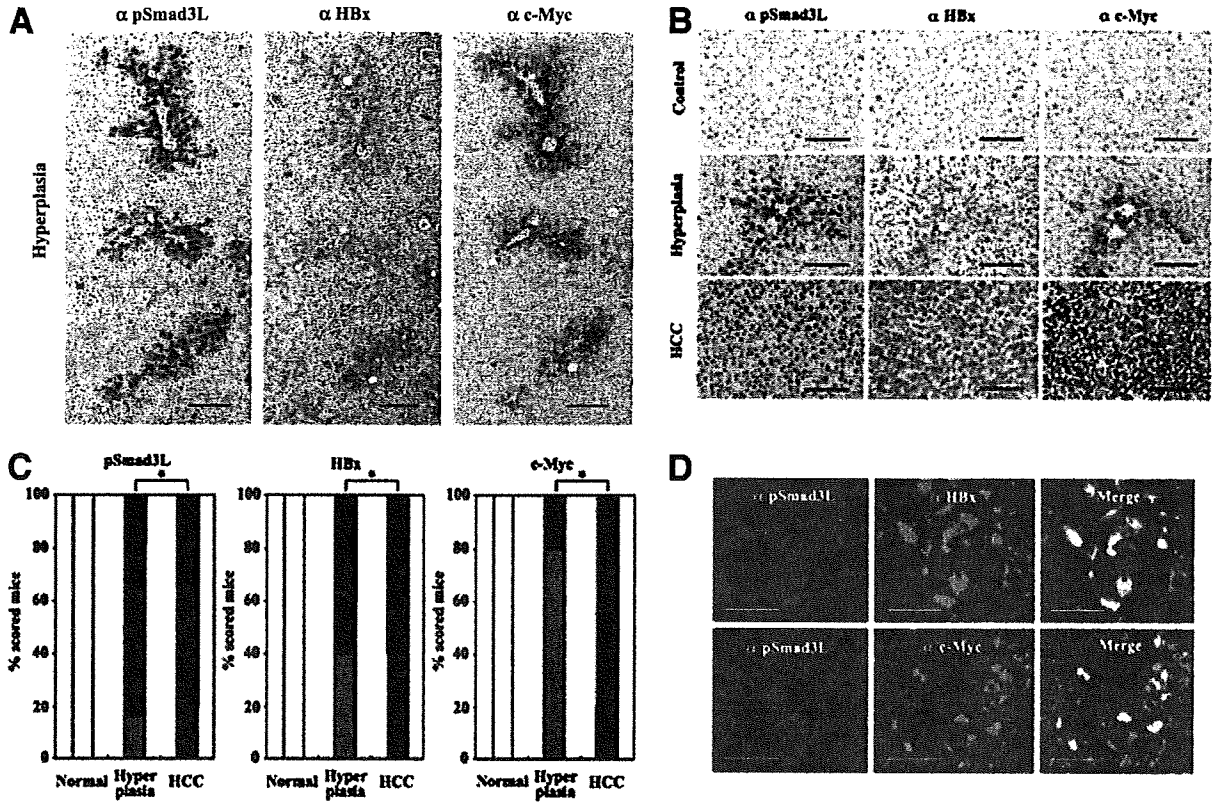

Fig. 6. The pSmad3L/c-Myc pathway was activated as HBx transgenic mouse liver progressed through hyperplasia to HCC. (A) Distribution of pSmad3L, HBx, and c-Myc in hyperplastic specimens from HBx transgenic mouse liver. (B) Distributions of pSmad3L, HBx, and c-Myc in normal liver, hyperplasia, and HCC specimens from HBx transgenic mice. Immunostaining for pSmad3L, HBx, and c-Myc was present in hyperplastic hepatocytes surrounding central veins in HBx transgenic mouse liver [(A) and (B), hyperplasia panels], and was distributed diffusely in HCC specimens [(B), HCC panel]. All sections were counterstained with hemotoxylin (blue). Brown color indicates specific Ab reactivity. Bar = 50 μm. (C) Hepatocytic pSmad3L, HBx, and c-Myc increased as HBx transgenic mouse liver progressed from hyperplasia to HCC. Staining for pSmad3L, HBx, and c-Myc was detected minimally in normal mouse livers, but was strongly up-regulated in neoplastic livers. In HCC, pSmad3L, HBx, and c-Myc were significantly greater than in livers with hyperplasia. *$P < 0.05$. Extent of pSmad3L, HBx, and c-Myc: □, 0; □, 1; ■, 2; ■, 3; ■, 4. (D) Hepatocytic pSmad3L in hyperplastic specimens from HBx transgenic mouse liver was colocalized with HBx and c-Myc. Hyperplasia sections of HBx transgenic mouse livers were stained for immunofluorescence to simultaneously detect pSmad3L (red) and HBx or c-Myc (green). Yellow color indicates overlap of proteins. Hepatocytes immunoreactive for pSmad3L showed colocalization of HBx (upper column) and c-Myc (lower column). Bar = 50 μm.

of HCC.[32] In contrast, HCC occasionally develops in healthy HBV surface antigen carriers, who are persistently infected with HBV but have normal liver function parameters and no necroinflammation.[33] This indicates that HBV itself has a direct influence on hepatocarcinogenesis in early chronic hepatitis B. Although integration of the viral genome into chromosomal DNA has not been reported in patients with HCV infection, integration of HBV has been detected in almost all cases of chronic hepatitis B,[3] leading to activation of the HBx-mediated oncogenic pathway.[4] It is noteworthy that HCC developed in patient 10 (Table 2), who showed strong pSmad3L positivity of hepatocytic nuclei but had minimal necroinflammatory activity (A1) or fibrosis (F1). In summary, HCV contributes indirectly to the development of HCC through chronic inflammation in early chronic hepatitis C. In contrast, HBV directly triggers the JNK/pSmad3L oncogenic pathway in early chronic hepatitis B, thus playing a role beyond mere stimulation of the host immune response.

Our findings also open up a new avenue to understanding the development and progression of hepatic fibrogenesis.[34] Whereas HSCs have traditionally been considered as the principal source of liver fibrosis, mature hepatocytes can acquire a mesencymal phenotype and perform the functions of activated HSC—that is, they can contribute to fibrogenesis.[35,36] In support of this notion, pSmad3L-mediated signaling promotes liver fibrosis by hepatocytes as well as activated HSCs during long-standing carcinogenesis.[13,18,20] In this manner, either HBV- or HCV-related chronic hepatitis progresses through fibrogenesis to HCC.

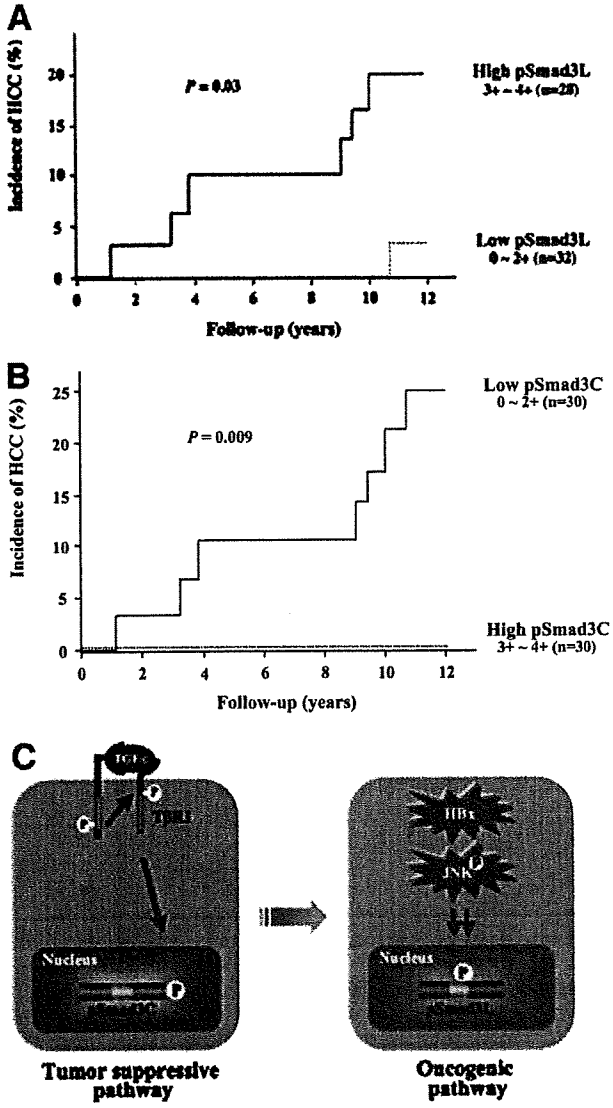

Fig. 7. Chronic hepatitis B patients with hepatocytes positive for pSmad3L and negative for pSmad3C increased risk of HCC development. (A) HCC occurred subsequently among patients whose hepatocytes in chronic hepatitis B specimens were strongly positive for pSmad3L. Incidence of HCC was significantly higher in patients with abundant Smad3L phosphorylation (scores 3 to 4, solid line) in hepatocytic nuclei versus those with sparse Smad3L phosphorylation (scores 0 to 2, dotted line). (B) HCC did not occur subsequently among patients whose hepatocytes in chronic hepatitis B specimens were strongly positive for pSmad3C. HCC occurred only in patients with sparse Smad3C phosphorylation (scores 0 to 2, solid line) in hepatocytic nuclei, while no patients with abundant Smad3C phosphorylation (scores 3 to 4, dotted line) have developed HCC. Cumulative rates of HCC occurrence from chronic hepatitis B were compared between cases with high and low phosphorylation of Smad3L and Smad3C (Kaplan-Meier analysis and log-rank test). (C) HBx protein shifted hepatic TGF-β signaling from the tumor-suppressive pSmad3C pathway to the oncogenic JNK-dependent pSmad3L pathway in early stages of chronic hepatitis B. Normal hepatocytes exhibited TGF-β-dependent Smad3 phosphorylation at the C-terminal region, which is related to growth inhibition by up-regulation of $p21^{WAF1}$. HBx protein activates JNK, promoting the oncogenic pSmad3L signaling, which fosters cell growth by up-regulating c-Myc, in a mean time reducing tumor-suppressive pSmad3C-mediated signaling.

The general biomedical approach to HCC is shifting away from population risk assessment and empirical treatment of patients to predictive personalized medicine based on molecular classification and targeted therapy.[29] Better knowledge of the risk factors associated with the occurrence of HCC can improve the effectiveness of surveillance programs. Our approach has identified pSmad3L and pSmad3C as prognostic markers that may prove to be clinically useful. Such predictive markers could allow us to select patients with chronic hepatitis B who have a high or low risk of developing HCC. Although the latter group could be followed up on an annual basis, the patients with a high risk require targeted surveillance measures to allow early diagnosis of HCC.

Phosphorylation of many transcription factors is controlled by the dynamic interplay between kinases and phosphatases. In this regard, we studied the kinetics of both linker and C-terminal phosphorylation of Smad3 in parental and HBx-expressing hepatocytes in response to TGF-β (unpublished observation). In parental hepatocytes, the levels of linker and C-terminal phosphorylation peaked at 30 minutes after the start of exposure to TGF-β and then gradually declined. However, HBx-expressing hepatocytes showed constitutive phosphorylation at Smad3L during continuous exposure to TGF-β. Several lines of evidence have identified small C-terminal domain phosphatase (SCP1-3) and protein phosphatase magnesium 1A (PPM1A) as the linker and C-terminal phosphatases, respectively.[37,38] Accordingly, SCP1-3 and PPM1A may reverse domain-specific phosphorylation in normal hepatocyes. In contrast, HBx-expressing hepatocytes may not show induction or activation of SCP1-3. Alternatively, linker phosphorylation in HBx-expressing hepatocytes might be resistant to SCP1-3.

Many researchers have been seeking key transcription factors regulating tumor-suppressive pathways that are altered in cancer. Our current model of JNK/pSmad3L signaling during HBV-related chronic liver disease suggests that specific inhibitors of the JNK/pSmad3L pathway might inhibit the progression of HCC. With respect to molecular targeting therapy for human HCC, pSmad3L and pSmad3C should be assessed as biomarkers to evaluate the benefit from specific inhibition of the JNK/pSmad3L pathway.

Acknowledgment: We thank Dr. Rik Derynck (University of California at San Francisco) and Dr. Seishi Murakami (Kanazawa University) for providing us with complementary DNAs encoding human Smad3 and HBx. We also thank Chiaki Kitano for assistance to construct ecotropic retrovirus and Natsuko Ohira for assistance with immunoblotting.

Table 5. Variables with Independent Predictive Value for HCC in Univariate and Multivariate Analyses

Characteristics	n	No. of Patients with HCC (%)	Univariate Analysis		Multivariate Analysis	
			Hazard Ratio (95% CI)	P Value	Hazard Ratio (95% CI)	P Value
pSmad3L positivity*						
Low (1 and 2)	32	1 (3)	1.00		1.00	
High (3 and 4)	28	6 (21)	3.8 (1.4-10.6)	0.01	14.8 (1.8-118.5)	0.01
pSmad3C positivity*						
High (3 and 4)	30	0 (0)	1.00		1.00	
Low (1 and 2)	30	7 (23)	2.8 (0.001-7.0)	0.03	16.4 (1.0-125.0)	0.04
Fibrotic stage†						
Low (F1 and F2)	39	4 (10)	1.00		1.00	
High (F3)	21	3 (14)	1.9 (0.7-5.4)	0.24	3.9 (0.4-38.6)	0.24
Inflammatory activity†						
Low (A0 and A1)	23	1 (4)	1.00		1.00	
High (A2 and A3)	37	6 (16)	1.8 (0.7-4.8)	0.27	0.2 (0.02-1.1)	0.06
HBV DNA (copies /mL)						
$<10^5$	42	3 (7)	1.00		1.00	
$>10^5$	18	4 (22)	1.9 (1.0-3.5)	0.05	2.5 (0.9-6.9)	0.08
HBeAg						
Negative	42	4 (10)	1.00		1.00	
Positive	18	3 (17)	2.1 (0.5-9.5)	0.32	9.9 (1.1-89.3)	0.03

Abbreviations: CI, confidence interval; HBeAg, hepatitis B e antigen; HBV, hepatitis B virus; HCC, hepatocellular carcinoma; pSmad3C, C-terminally phosphorylated Smad3; pSmad3L, linker-phosphorylated Smad3.

*Hepatocytic Smad3 phosphorylation in chronic hepatitis B specimens is scored as follows: 0, no phosphorylation; 1, <25% Smad3 phosphorylation; 2, 25% to 50% Smad3 phosphorylation; 3, 50% to 75% Smad3 phosphorylation; 4, >75% Smad3 phosphorylation.

†Necroinflammatory activity and fibrotic stage are determined histologically according to Desmet's classification.

References

1. Llovet JM, Burroughs A, Bruix J. Hepatocellular carcinoma. Lancet 2003; 362:1907-1917.
2. El-Serag HB. Hepatocellular carcinoma: recent trends in the United States. Gastroenterology 2004;127(Suppl):27S–34S.
3. Brechot C, Pourcel C, Louise A, Rain B, Tiollais P. Presence of integrated hepatitis B virus DNA sequences in cellular DNA of human hepatocellular carcinoma. Nature 1980;286:533-535.
4. Kim CM, Koike K, Saito I, Miyamura T, Jay G. HBx gene of hepatitis B virus induces liver cancer in transgenic mice. Nature 1991;351:317-320.
5. Yu DY, Moon HB, Son JK, Jeong S, Yu SL, Yoon H, et al. Incidence of hepatocellular carcinoma in transgenic mice expressing the hepatitis B virus X-protein. J Hepatol 1999;31:123-132.
6. Koike K, Moriya K, Iino S, Yotsuyanagi H, Endo Y, Miyamura T, et al. High-level expression of hepatitis B virus HBx gene and hepatocarcinogenesis in transgenic mice. HEPATOLOGY 1994;19:810-819.
7. Benn J, Su F, Doria M, Schneider RJ. Heptitis B virus HBx protein induces transcription factor AP-1 by activation of extracellular signal-related and c-Jun N-terminal mitogen-activated protein kinases. J Virol 1996;70: 4978-4985.
8. Roberts AB, Sporn MB. The transforming growth factor-βs. In: Sporn MB, Roberts AB, eds. Peptide Growth Factors and Their Receptors. Berlin: Springer-Verlag, 1990:419-472.
9. Heldin CH, Miyazono K, ten Dijke P. TGF-β signaling from cell membrane to nucleus through SMAD proteins. Nature 1997;390:465-471.
10. Massagué J. TGF-β signal transduction. Annu Rev Biochem 1998;67: 753-791.
11. Kretzschmar M, Doody J, Timokhina I, Massague J. A mechanism of repression of TGF-β/Smad signaling by oncogenic Ras. Genes Dev 1999; 13:804-816.
12. Mori S, Matsuzaki K, Yoshida K, Furukawa F, Tahashi Y, Yamagata H, et al. TGF-β and HGF transmit the signals through JNK-dependent Smad2/3 phosphorylation at the linker regions. Oncogene 2004;23:7416-7429.
13. Furukawa F, Matsuzaki K, Mori S, Tahashi Y, Yoshida K, Sugano Y, et al. p38 MAPK mediates fibrogenic signal through Smad3 phosphorylation in rat myofibroblasts. HEPATOLOGY 2003;38:879-889.
14. Matsuura I, Denissova NG, Wang G, He D, Long J, Liu F. Cyclin-dependent kinases regulate the antiproliferative function of Smads. Nature 2004;430:226-231.
15. Yamagata H, Matsuzaki K, Mori S, Yoshida K, Tahashi Y, Furukawa F, et al. Acceleration of Smad2 and Smad3 phosphorylation via c-Jun NH(2)-terminal kinase during human colorectal carcinogenesis. Cancer Res 2005; 65:157-165.
16. Sekimoto G, Matsuzaki K, Yoshida K, Mori S, Murata M, Seki T, et al. Reversible Smad-dependent signaling between tumor suppression and oncogenesis. Cancer Res 2007;67:5090-5096.
17. Arany PR, Rane SG, Roberts AB. Smad3 deficiency inhibits v-ras-induced transformation by suppression of JNK MAPK signaling and increased farnesyl transferase inhibition. Oncogene 2008;27:2507-2512.
18. Yoshida K, Matsuzaki K, Mori S, Tahashi Y, Yamagata H, Furulawa F, et al. Transforming growth factor-β and platelet-derived growth factor signal via c-Jun N-terminal kinase-dependent Smad2/3 phosphorylation in rat hepatic stellate cells after acute liver injury. Am J Pathol 2005;166:1029-1039.
19. Block TM, Mehta AS, Fimmel CJ, Jordan R. Molecular viral oncology of hepatocellular carcinoma. Oncogene 2003;22:5093-5107.
20. Matsuzaki K, Murata M, Yoshida K, Sekimoto G, Uemura Y, Sakaida N, et al. Chronic inflammation associated with hepatitis C viral infection perturbs hepatic TGF-β signaling, promoting cirrhosis and hepatocellular carcinoma. HEPATOLOGY 2007;46:48-57.
21. Desmet VJ, Gerber M, Hoofnagle JH, Manns M, Scheuer PJ. Classification of chronic hepatitis: diagnosis, grading and staging. HEPATOLOGY 1994;19:1513-1520.
22. Cox DR. Regression models and life-tables. J R Stat Soc (B) 1972;34:187-220.
23. Pardali K, Moustakas A. Actions of TGF-β as tumor suppressor and pro-metastatic factor in human cancer. Biochim Biophys Acta 2007;1775:21-62.

24. Chen CJ, Yang HI, Su J, Jen CL, You SL, Lu SN, et al. REVEAL-HBV study group. Risk of hepatocellular carcinoma across a biological gradient of serum hepatitis B virus DNA level. JAMA 2006;295:65-73.
25. Feitelson MA. c-Myc overexpression in hepatocarcinogenesis. Human Pathology 2004;35:1299-1302.
26. Yang HI, Lu SN, Liaw YF, You SL, Sun CA, Wang LY, et al. Taiwan community-based cancer screening project group. Hepatitis B e antigen and the risk of hepatocellular carcinoma. N Engl J Med 2002;347:168-174.
27. Thorgeirsson SS, Lee JS, Grisham JW. Functional genomics of hepatocellular carcinoma. HEPATOLOGY 2006;43:145-150.
28. Theise ND, Park YN, Kojiro M. Dysplastic nodules and hepatocarcinogenesis. Clin Liver Dis 2002;6:497-512.
29. Thorgeirsson SS, Grisham JW. Molecular pathogenesis of human hepatocellular carcinoma. Nat Genet 2002;31:339-346.
30. Chisari FV, Klopchin K, Moriyama T, Pasquinelli C, Dunsford HA, Sell S, et al. Molecular pathogenesis of hepatocellular carcinoma in hepatitis B virus transgenic mice. Cell 1989;59:1145-1156.
31. Moriya K, Fujie H, Shintani Y, Yotsuyanagi H, Tsutsumi T, Ishibashi K, et al. The core protein of hepatitis C virus induces hepatocellular carcinoma in transgenic mice. Nat Med 1998;4:1065-1067.
32. Di Bisceglie AM. Hepatitis C and hepatocellular carcinoma. HEPATOLOGY 1997;26 (Suppl):34S–38S.
33. Popper H, Shafritz DA, Hoofnagle JH. Relation of the hepatitis B virus carrier state to hepatocellular carcinoma. HEPATOLOGY 1987;7:764-772.
34. Inagaki Y, Okazaki I. Emerging insights into transforming growth factor β Smad signal in hepatic fibrogenesis. Gut 2007;56:284-292.
35. Kaimori A, Potter J, Kaimori JY, Wang C, Mezey E, Koteish A. Transforming growth factor-β1 induces an epithelial-to-mesenchymal transition state in mouse hepatocytes in vitro. J Biol Chem 2007;282:22089-22101.
36. Weng HL, Ciuclan L, Liu Y, Hamzavi J, Godoy P, Gaitantzi H, et al. Profibrogenic transforming growth factor-β/activin receptor-like kinase 5 signaling via connective tissue growth factor expression in hepatocytes. HEPATOLOGY 2007;46:1257-1270.
37. Lin X, Duan X, Liang YY, Su Y, Wrighton KH, Long J, et al. PPM1A functions as a Smad phosphatase to terminate TGFβ signaling. Cell 2006; 125:915-928.
38. Wrighton KH, Willis D, Long J, Liu F, Lin X, Feng XH. Small C-terminal domain phosphatases dephosphorylate the regulatory linker regions of Smad2 and Smad3 to enhance transforming growth factor-β signaling. J Biol Chem 2006;281:38365-38375.

THE JOURNAL OF BIOLOGICAL CHEMISTRY VOL. 284, NO. 6, pp. 3513–3520, February 6, 2009

A Single Amino Acid of Toll-like Receptor 4 That Is Pivotal for Its Signal Transduction and Subcellular Localization*

Received for publication, April 22, 2008, and in revised form, October 29, 2008 Published, JBC Papers in Press, December 8, 2008, DOI 10.1074/jbc.M803086200

Shintaro Yanagimoto[‡§¶], Keita Tatsuno[§], Shu Okugawa[§], Takatoshi Kitazawa[§], Kunihisa Tsukada[§], Kazuhiko Koike[§], Tatsuhiko Kodama[¶], Satoshi Kimura[‖], Yoshikazu Shibasaki[‡1], and Yasuo Ota[1,2]**

*From the [‡]Center for Structuring Life Sciences, Graduate school of Arts and Sciences, University of Tokyo, Meguro-ku, Tokyo 153-8903, the [§]Department of Infectious Diseases, Graduate School of Medicine, University of Tokyo, Bunkyo-ku, Tokyo 113-8655, the [¶]Laboratory for Systems Biology and Medicine, Research Center for Advanced Science and Technology, University of Tokyo, Meguro-ku, Tokyo 153-8904, the [‖]Tokyo Teishin Hospital, Fujimi, Chiyoda-ku, Tokyo 102-8798, and the **Department of Medicine, Teikyo University School of Medicine, 2-11-1, Kaga, Itabashi-ku, Tokyo 173-8605, Japan*

Toll-like receptor 4 (TLR4) is essential for recognizing a Gram-negative bacterial component, lipopolysaccharide (LPS). A single amino acid mutation at position 712 of murine TLR4 leads to hyporesponsiveness to LPS. In this study we determined that an amino acid, a leucine at position 815 of human TLR4, is also pivotal for LPS responsiveness and subcellular distribution. By replacing the leucine with alanine, the mutant TLR4 lost responsiveness to LPS and did not localize on the plasma membrane. In addition, it does not coprecipitate with myeloid differentiation-2, an accessory protein that is necessary for TLR4 to recognize LPS. These results suggest that the leucine at position 815 is required for the normal maturation of TLR4 and for formation of the TLR4·MD-2 complex.

Toll-like receptors (TLRs)[3] play essential roles in both innate and adaptive immunity (1). Thirteen members of the TLR family have been identified in mammals. TLRs have leucine-rich-repeats in their extracellular domains and a Toll/Interleukin-1 receptor (TIR) in their cytoplasmic domains, the latter of which mainly mediates intracellular signaling. Signaling pathways of TLRs, except for TLR3, depend on an adapter protein, MyD88 (myeloid differentiation factor 88), which interacts with the TIR domain of TLRs. This pathway leads to the activation of the transcription factor NF-κB and production of cytokines such as tumor necrosis factor-α and interleukin-6. Another important signaling pathway mediated by TLR3 and TLR4 that exploits the TIR domain is the MyD88-independent pathway. This pathway involves different adapter proteins, such as the TIR domain-containing adaptor inducing interferon-β (TRIF) and TRIF-related adaptor molecule (2–4), and is essential for production of type I interferon through activation of interferon regulatory factor-3.

TLRs recognize as ligands several microbial pathogen-associated molecular patterns. One such pathogen-associated molecular pattern is lipopolysaccharide (LPS), which is recognized by TLR4. LPS triggers severe immunologic reactions by the host in Gram-negative bacterial infections and has drawn attention in many clinical situations. TLR4 is the first mammalian TLR to be discovered in the context of immunology. TLR4 was identified in the search for the genes responsible for LPS hyporesponsiveness (5, 6). The defect was found to stem from a single amino acid mutation, replacement of proline with histidine at position 712, in the cytoplasmic tail of murine TLR4. The study led to the discovery of the importance of TLR4 in innate immunity.

A variety of cells are activated by LPS stimulation through TLR4. TLR4 forms a receptor complex with an accessory protein, myeloid differentiation-2 (MD-2). MD-2 first associates with TLR4 in the endoplasmic reticulum (ER) and *cis*-Golgi, and both proteins move together to the plasma membrane (7, 8). Upon recognition of LPS, the TLR4·MD-2 complex receives LPS on the cell surface and initiates intracellular signaling. The expression of TLR4 in the absence of MD-2 does not confer full responsiveness to LPS stimuli in experimental cell lines (9). An analysis of MD-2 knockout mice revealed that MD-2 is important not only for LPS sensing but also for cellular distribution of TLR4.

In this study we hypothesized that the cytoplasmic tail of TLR4 contains regions that control both localization and signaling. Using truncation and mutation analysis, and paying particular attention to the TIR domain, we identified a single amino acid that is pivotal for both TLR4 signaling and subcellular distribution. The site we found was on the C-terminal portion of the TIR domain for which no specific function has been yet determined.

* This work was partly supported by the Program of Fundamental Studies in Health Sciences of the National Institute of Biomedical Innovation, by the Focus 21 project of the New Energy and Industrial Technology Development Organization, and by the Special Coordination Fund for Science and Technology from the Ministry of Education, Culture, Sports, Science and Technology. This study was also partly supported by a grant-in-aid from the Ministry of Education, Culture, Sports, Science and Technology (to Y. O.). The costs of publication of this article were defrayed in part by the payment of page charges. This article must therefore be hereby marked "*advertisement*" in accordance with 18 U.S.C. Section 1734 solely to indicate this fact.

[1] Both authors contributed equally to this work.

[2] To whom correspondence should be addressed. Tel.: 81-3-3964-1211 (ext. 1756); Fax: 81-3-3579-6310; E-mail: yasuota-tky@umin.ac.jp.

[3] The abbreviations used are: TLR, Toll-like receptor; TIR, Toll/Interleukin-1 receptor; TRIF, TIR domain-containing adaptor inducing interferon-β; LPS, lipopolysaccharide; MD-2, myeloid differentiation-2; ER, endoplasmic reticulum; GFP, green fluorescent protein; EGFP, enhanced GFP; RLA, relative luciferase activity; Sulfo-NHS-SS-Biotin, sulfosuccinimidyl-2-(biotinamido)ethyl-1,3-dithiopropionate.

EXPERIMENTAL PROCEDURES

Reagents and Other Materials—Lipopolysaccharide (LPS) from *Escherichia coli* O55:B5 was purchased from Sigma-Aldrich and applied without repurification. FLAG- and hexa-histidine (His_6)-tagged human TLR4 expression plasmid (pEFBOS/humanTLR4flaghis) and FLAG- and His_6-tagged human MD-2 expression plasmid (pEFBOS/humanMD-2flaghis) were generous gifts from Dr. Kensuke Miyake (Institute of Medical Science, University of Tokyo, Japan). Human CD14 cDNA plasmid (pCMV6-XL5/humanCD14) was purchased from OriGene (Rockville, MD). Fluorescent protein expression vector pEGFP-N3 was purchased from Clontech (Mountain View, CA). Anti-TLR4 monoclonal antibody (clone HTA125) was purchased from Abcam (Cambridge, MA). Anti-FLAG monoclonal antibody (clone M2) was purchased from Sigma-Aldrich. Anti-*A.v.* (GFP) monoclonal and polyclonal antibodies were purchased from Clontech. Control immunoglobulins for immunoprecipitation were purchased from BD Biosciences (San Jose, CA). Horseradish peroxidase-labeled anti-immunoglobulins antibodies were purchased from Dako (Glostrup, Denmark). BlockAce (DS Pharma Biomedical, Osaka, Japan) solution was used as blocking buffer for Western blotting.

Cell Culture—Human embryonic kidney (HEK) 293T cells were maintained in Dulbecco's modified Eagle's medium (Sigma-Aldrich) containing 10% heat-inactivated fetal bovine serum supplemented with penicillin-streptomycin solution (Invitrogen). FuGENE 6 transfection reagent (Roche Applied Science) was used for transient cotransfection according to the manufacturer's instructions. Culture dishes or plates were prepared to 70% confluence prior to transfection. Cells were used for experiments 36 h later. The transfection conditions were optimized for microscopic observation of the expressed fluorescent protein and were kept unchanged in other experiments.

Expression Vector Subcloning and Mutagenesis—Wild-type TLR4 cDNA was excised from pEFBOS/humanTLR4flaghis and subcloned into pEGFP-N3 so that when expressed enhanced green fluorescent protein (EGFP) would be fused at the C terminus of TLR4 (pEGFP-N3/humanTLR4). All mutations were introduced into pEFBOS/humanTLR4flaghis and pEGFP-N3/humanTLR4 using the QuikChange site-Directed mutagenesis kit (Stratagene, La Jolla, CA) according to the manufacturer's instructions and were confirmed by sequencing. For the truncation analysis, two identical unique restriction sites were prepared in the TLR4-coding region of pEFBOS/humanTLR4 using a QuikChange kit, and the DNA fragment to be removed, which was a part of the C terminus of TLR4, was excised enzymatically. After agarose gel purification, the linear double-stranded DNA was ligated to re-form a circular plasmid. Restriction sites were designed so as not to cause a frameshift between TLR4 and EGFP.

Confocal Laser Scanning Microscopy of Cells—Samples were fixed in 3% paraformaldehyde-phosphate-buffered saline at 37 °C for 10 min. Fluorescence images of fixed samples were recorded using a FluoView FV1000 Confocal Microscope (an inverted confocal laser scanning microscope, Olympus, Tokyo, Japan).

Immunoprecipitation—Transfected cells were lysed in lysis buffer (50 mM Tris-HCl, pH 7.5, 100 mM NaCl, 0.1% Triton X-100, 1 mM 1,4-dithiothreitol, and proteinase inhibitor mixture), sonicated, and centrifuged at 4 °C. Antibody was added to the supernatant, and the sample was rotated 1 h at 4 °C followed by the addition of protein G-Sepharose (GE Healthcare Life Sciences, Piscataway, NJ) and an additional 8-h incubation at 4 °C. Bound protein was washed three times in lysis buffer. Proteins were eluted by boiling in SDS sample buffer.

Biotinylation and Purification of Cell Surface Proteins—Prior to surface biotinylation, HEK 293T cells plated in a 100-mm dish were transiently transfected as described above. Surface biotinylation and subsequent purification of biotinylated proteins were performed using a Cell Surface Protein Biotinylation and Purification Kit (Pierce) following the manufacturer's instructions. Briefly, membrane-impermeable sulfosuccinimidyl-2-(biotinamido)ethyl-1,3-dithiopropionate (Sulfo-NHS-SS-Biotin) was added to cell monolayers in the culture dishes and covalently bound to amines in proteins exposed on the cell surface. The affinity resin that binds to the biotin end of Sulfo-NHS-SS-Biotin was used to collect the biotinylated proteins. Reduction by 1,4-dithiothreitol causes cleavage of the disulfide bond in Sulfo-NHS-SS-Biotin, and the elute contains the biotinylated cell surface proteins. Each final sample obtained was considered to contain proteins from an equal amount of cells, because all culture plates were treated equally and grown to full confluence. All samples were sonicated and subjected to SDS-PAGE and Western blotting. The membrane to which protein was transferred was blocked in blocking buffer for 1 h. Then the membrane was incubated with a primary antibody, followed by incubation with horseradish peroxidase-labeled anti-immunoglobulins antibody. The protein bands were then visualized by using a chemiluminescence reagent, Immobilon Western Chemiluminescent HRP Substrate (Millipore, Billerica, MA), according to the manufacturer's instructions.

Cell Stimulation Assays—HEK293T cells were plated and transiently transfected for assays. Thirty-six hours after the transfection, LPS was added to fresh culture medium in each well of the culture plates at the stated concentration. The duration of LPS stimulation was 7 h.

Dual Luciferase Reporter Assays for NF-κB Activation—HEK293T cells were plated in 12-well culture plates (4×10^4 cells/well), and experimental cDNA plasmids were transiently transfected 36 h later using the FuGENE 6 transfection reagent with 0.5 μg of NF-κB reporter plasmid expressing firefly luciferase (pNF-κB-Luc, Stratagene) and 0.05 μg of constitutively active *Renilla* luciferase reporter plasmid (pRL-TK, Promega, Madison, WI) in addition to 0.5 μg each of TLR4-EGFP plasmid and MD-2 plasmid. Stimulation experiments were performed 36 h later. Firefly luciferase and *Renilla* luciferase activities were measured using the Dual-Luciferase Reporter Assay System (Promega) and the Genelight55 luminometer (Microtech, Chiba, Japan). Relative luciferase activity (RLA) was obtained as the ratio of firefly luciferase activity to *Renilla* luciferase activity. Results are expressed as the ratio of RLA with LPS stimulation to RLA without LPS stimulation ([RLA LPS+]/[RLA LPS−]). This ratio should ideally approach 1 when no response to LPS stimulation is observed.

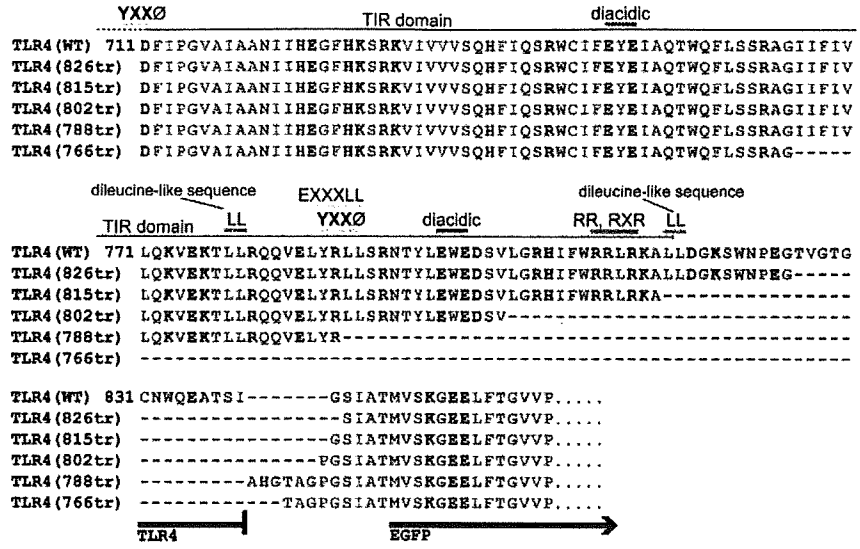

FIGURE 1. **Alignment of the cytoplasmic domains of EGFP fusion TLR4 truncation mutants used in this study.** TLR4 (766tr) signifies the mutant truncated at position 766. Others are named in the same manner. The amino acids are colored based on their physicochemical properties: *pink*, basic; *blue*, acidic; *green*, polar and neutral; and *orange*, hydrophobic. The *black overline* represents the TIR domain. *Colored overlines* indicate amino acid sequences identical to known sorting signal motifs except for two LLs, which are dileucine motif-like sequences in that they consist of solely two consecutive leucines without preceding aspartate or glutamate. *Capital letters* on the *line* signify the single-letter code for amino acids: *E*, glutamic acid; *L*, leucine; *R*, arginine; and *Y*, tyrosine. *X* signifies any amino acid, and Ø signifies an amino acid residue with a bulky hydrophobic side chain.

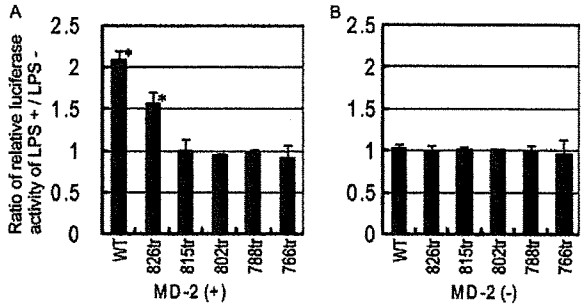

FIGURE 2. **LPS responsiveness measured by NF-κB luciferase assay.** HEK293T cells were transfected with plasmids containing the gene for wild-type TLR4 or a truncated human TLR4-EGFP fusion protein, in addition to a luciferase reporter and human MD-2 plasmid (*A*) or unmodified plasmids (control) (*B*). After 36 h, cells were stimulated with LPS (10 ng/ml) for 7 h, and luciferase reporter gene activity was measured. All results were expressed as the ratio of relative luciferase activity with LPS stimulation to that without stimulation. The data were from three independent experiments. *Small bars* indicate 95% confidence intervals of the mean (*p* values for * are: TLR4 (WT)-EGFP/MD-2 (+), $p = 0.002$; TLR4 (826tr)-EGFP/MD-2 (+), $p = 0.016$).

Statistical Analyses—All quantitative experiments were repeated three times, and each experiment was done in triplicate. The ratio of relative luciferase activity of LPS+ to LPS− was calculated as the index of the responsiveness to the stimuli as explained above. When positive response is observed, the ratio should significantly exceed one. The means of the ratio were represented in *bar graphs*. The 95% confidence interval of the mean of the ratio was calculated and indicated on each *bar* in the *graph*, and *p* values were calculated using Student's *t* distribution compared with the hypothetical mean, one.

RESULTS

Truncation Analysis of TLR 4—To identify amino acid sequences in the cytoplasmic tail of TLR4 that are involved in both signal transduction and subcellular distribution, first we generated five truncation mutants of TLR4 with a fluorescent protein (EGFP) at the C terminus of TLR4.

Although there are no known definite sorting signal motifs in the cytoplasmic tail of TLR4, some amino acid sequences are similar or identical to known general sorting signal motifs as shown in Fig. 1. *YXXØ*, a form of tyrosine-based sorting signal, and *EXXXLL*, a form of dileucine (LL)-based sorting signal, both control protein internalization, lysosomal targeting, and basolateral targeting (10), where "*X*" represents any amino acid, "*Ø*" stands for an amino acid residue with a bulky hydrophobic side chain, and other letters are single-letter abbreviations for the amino acids. "Diacidic" signals such as D*X*E mediate export from the ER (11). RR or R*X*R is another example of an ER export signal (12). Truncation sites were chosen so that some of these amino acid sequences were deleted in each mutant. Because the TIR domain, which is essential in TLR4 signaling and possibly subcellular localization (13), spans most of the cytoplasmic domain of TLR4, four out of five mutants have involvement in the TIR domain, which we hypothesized could result in impaired signal transduction and a change in subcellular distribution. Part of the cytoplasmic portion of the amino acid sequence of the truncation mutants is shown in Fig. 1. The five truncation mutant proteins lost their C-terminal tails at positions 826, 815, 802, 788, and 766, respectively, and were conjugated with EGFP *in vitro*. Actual truncation and ligation sites of all actual mutants were confirmed to have the designed DNA alignment by sequencing.

We utilized the luciferase reporter assay to assess NF-κB transcription activity as an indicator of TLR4 response to LPS stimuli. MD-2 is reported to be essential for this response (9). However, because it is not known whether MD-2 is necessary for transduction of the truncated TLR4 signal as well, we performed the assays with and without MD-2. The index of cell responsiveness to the stimulation was measured as the ratio between RLA with LPS stimulation and RLA without LPS stimulation. Only cells transfected with TLR4 (826tr)-EGFP in combination with MD-2 retained responsiveness to LPS stimulation. One exception was wild-type TLR4-EGFP (Fig. 2*A*). HEK293T cells transfected with TLR4 but without MD-2 did not respond to LPS stimuli regardless of the TLR4-EGFP genotype (Fig. 2*B*).

Next, we compared the localization of wild-type and truncated mutants of TLR4-EGFP in HEK293T by fluorescence microscopy (Fig. 3*A*). The wild-type TLR4 cotransfected with MD-2 was expressed on the plasma membrane and also in the

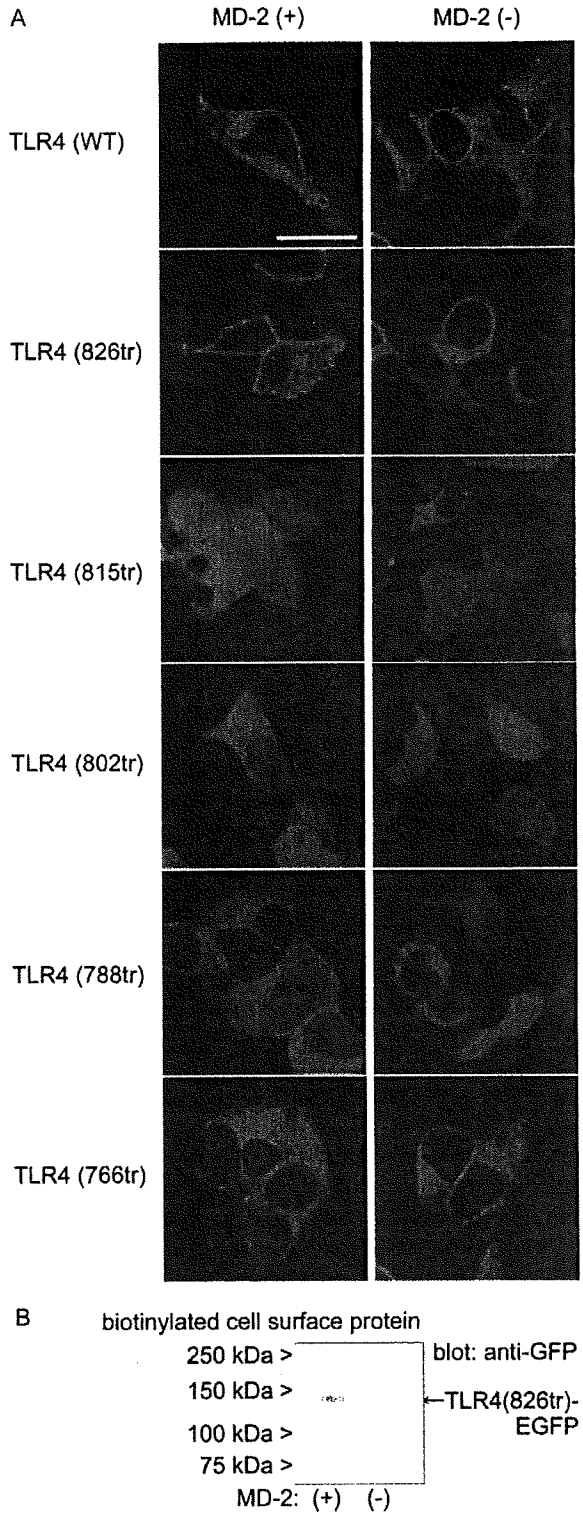

FIGURE 3. **Residues 815–826 of TLR4 contain a region necessary for plasma membrane localization.** *A*, cells were cultured on coverslips in 12-well plates and transfected as in Fig. 2. EGFP-tagged TLR4 was visualized by laser confocal microscopy. Fluorescence from EGFP was observed in *green*. Each genotype of TLR4-EGFP was cotransfected with a human MD-2 plasmid or empty vector. *Bar*, 20 μm. *B*, TLR4 (826tr)-EGFP with or without coexpression of MD-2 were tagged by biotinylation of the cell surface proteins and affinity-purified. TLR4 was visualized by immunoblotting using an anti-GFP monoclonal antibody. Samples from both combinations of DNAs were prepared from the same number of cells.

perinuclear area. These findings were consistent with observations by others (14, 15). TLR4 is reported to localize in the Golgi apparatus as well as on the plasma membrane. Our observation of TLR4-EGFP accumulation in the perinuclear area does not contradict the report that TLR4 partly localizes in the Golgi apparatus (14).

TLR4-EGFP truncation mutants, 815tr, 802tr, 788tr, and 766tr apparently did not localize at the plasma membrane. No particular fluorescence pattern that might be characteristic of localization to a specific intracellular compartment was observed. Only TLR4 (826tr)-EGFP, which has the shortest truncation, was expressed on the plasma membrane and in the perinuclear area, and the fluorescence pattern was similar to that of wild-type (Fig. 3*A*). No TLR4 genotypes, including wild-type TLR4-EGFP, clearly localized on the plasma membrane in the absence of MD-2 (Fig. 3*A*). MD-2 is reported to be necessary for localization of wild-type TLR4 at the plasma membrane (15), which is consistent with our observation. Intracellular distribution of mutant TLR4 varied depending on the genotype, but no particular cellular structure was identified as an alternative target site. Furthermore, we examined the plasma membrane expression of TLR4 (826tr)-EGFP by cell surface protein biotinylation. The expression level of TLR4 (826tr)-EGFP was markedly decreased without coexpression of MD-2 (Fig. 3*B*), which is compatible with the microscope observation.

Removal of the C-terminal segment of TLR4 at residue 826 does not qualitatively affect LPS responsiveness and subcellular distribution. However, when more residues, up to position 815, were removed, both signal transduction and plasma membrane localization were impaired. These results suggest that residues 815–826 of TLR4 contain at least one segment that is critical for those functions.

Amino Acid Sequence Replacement Analysis—To identify critical amino acid sequences in this region, we generated an amino acid replacement mutant of TLR4 instead of truncation mutants. As shown in Fig. 1, although it is not a canonical sequence, leucine-leucine at 815–816 partially fits a known sorting signal motif, a dileucine motif, (D/E)*XXX*L(L/I) or D*XX*LL, which plays an important role in internalization of plasma membrane protein or sorting from the *trans*-Golgi network (10). Thus, as has been done in a similar study (16), a mutant was generated in which alanines were substituted for both leucines at positions 815 and 816.

We measured the NF-κB activity of TLR4 (L815AL816A)-EGFP, the mutant in which both leucines were replaced with alanines, under LPS stimulation (Fig. 4*A*). This mutant protein did not respond to LPS stimuli. Microscopic observation revealed that TLR4 (L815AL816A)-EGFP was not expressed on the plasma membrane regardless of whether MD-2 was cotransfected (Fig. 4*B*). The phenotype of this doubly substituted mutant appeared to be the same as that of the truncation mutants. These results imply that the leucines in positions 815 and 816 play an important role in TLR4 plasma membrane localization.

Analysis of Single Amino Acid Substitution Mutants—As previously mentioned, the amino acid sequence leucine-leucine at positions 815 and 816 does not completely match the dileucine motif, *i.e.* it lacks a preceding acidic amino acid. Therefore it

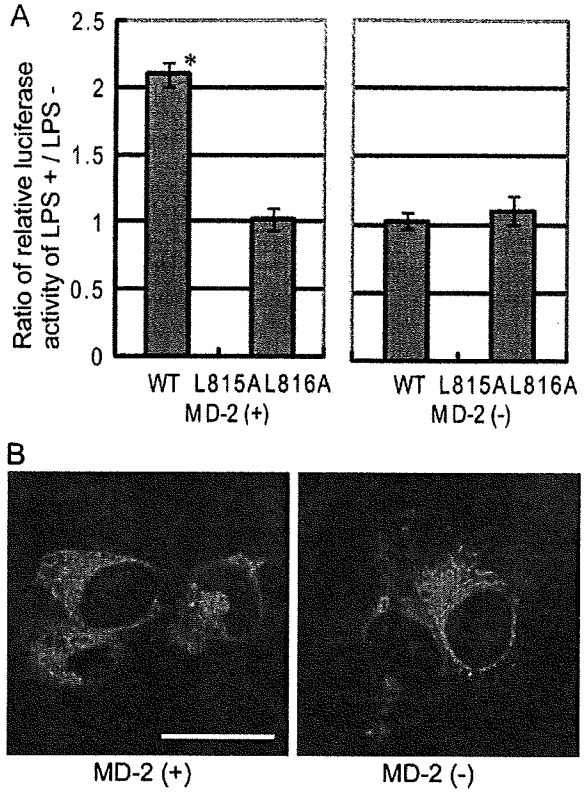

FIGURE 4. **Leucines at positions 815–816 of TLR4 are responsible for impairment of LPS responsiveness and plasma membrane expression.** *A*, the LPS stimulation assay was done for TLR4 (L815AL816A)-EGFP as in Fig. 2. The data were from three independent experiments. *Small bars* indicate 95% confidence intervals of the mean (*p* value for * are: TLR4 (WT)-EGFP/MD-2 (+), $p = 0.002$). *B*, TLR4 (L815AL816A)-EGFP expression in HEK293T cells was observed by laser confocal microscopy. *Bar*, 20 μm.

was reasonable to explore whether leucines 815 and 816 need to be adjacent to each other. We created five genotypes of single amino acid mutants of TLR4: TLR4 (K813A)-EGFP, TLR4 (L815A)-EGFP, TLR4 (L816A)-EGFP, and TLR4 (D817A)-EGFP. We excluded the amino acid at position 814 from the analysis, because the amino acid in position 814 of wild-type TLR4 is alanine. The amino acid sequence alignment of wild-type TLR4 and the single amino acid replacement mutants is shown in Fig. 5. DNA sequences were confirmed by sequencing.

As was done with truncation mutants, we measured NF-κB activity of wild-type TLR4-EGFP, TLR4 (K813A)-EGFP, TLR4 (L815A)-EGFP, TLR4 (L816A)-EGFP, and TLR4 (D817A)-EGFP in response to LPS stimulation. All mutants except TLR4 (L815A)-EGFP showed responsiveness to LPS stimulation with coexpression of MD-2 (Fig. 6*A*). Without MD-2, no genotype of TLR4-EGFP responded to LPS stimulation (Fig. 6*B*). LPS stimulation was performed in an identical manner as with truncation mutants.

We analyzed the subcellular distribution of single amino acid mutants of TLR4-EGFP with and without MD-2 coexpression by fluorescence microscopy. TLR4 (K813A)-EGFP and TLR4 (D817A)-EGFP showed a similar fluorescence pattern to the wild-type, which localized at the plasma membrane when coexpressed with MD-2. No genotypes of TLR4-EGFP localized on the plasma membrane without MD-2 (Fig. 7). The cells transfected with TLR4 (L815A)-EGFP coexpressed with MD-2 did not show plasma membrane fluorescent pattern. Also, TLR4 (L815A)-EGFP showed comparatively weaker fluoresce than other mutants, possibly due to lower expression of the protein. Fluorescence of TLR4 (L816A)-EGFP with MD-2 was ambiguous as for the plasma membrane expression. Some kind of membranous structure was observed in the cytoplasmic area, but the intensity of the plasma membrane green fluorescence was obscure. Together with the results from the LPS stimulation experiment, the leucines at positions 815 and 816 are considered to play important roles in signal transduction and/or subcellular distribution of TLR4.

Because EGFP consists of 239 amino acids, which is about one-third the size of the complete TLR4 protein, the experimental results obtained using TLR4-EGFP could have been influenced by the presence of the EGFP fused at the C terminus of TLR4. To rule out this possibility, we tested the functional integrity of both TLR4 (L815A) and TLR4 (L816A) with and without EGFP at the C terminus. Reporter assays were performed under the same conditions except that the shorter tag, FLAG-His_6, which has only 21-amino acid tags at the C terminus, was fused to TLR4 in place of EGFP. There was no difference

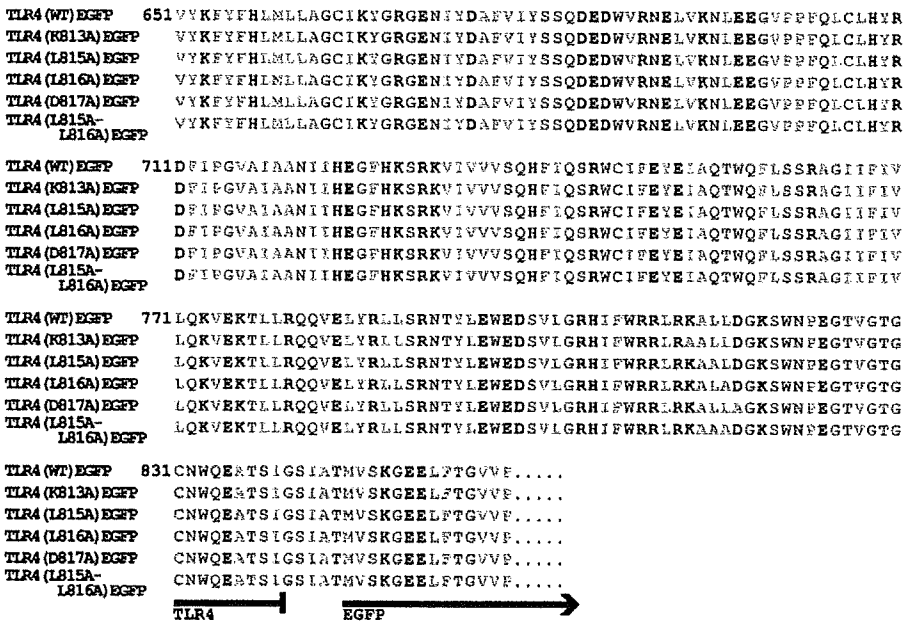

FIGURE 5. **Alignment of the cytoplasmic domain of EGFP fusion TLR4 amino acid-replacement mutants used in this study.** TLR4 (L813A) signifies a mutant with leucine replaced with alanine at position 813. Others are named in the same manner. The amino acids are *colored* as in Fig. 1. All amino acids are designated using the single-letter code.